Precambrian Research 304 (2018) 125–139

Contents lists available at ScienceDirect

Precambrian Research

journal homepage: www.elsevier.com/locate/precamres

SIMS microanalysis of the Strelley Pool Formation cherts and the implications for the secular-temporal oxygen-isotope trend of cherts

J.N. Cammack[a,f,g,*], M.J. Spicuzza[a,f], A.J. Cavosie[a,e], M.J. Van Kranendonk[b], A.H. Hickman[c], R. Kozdon[a,d,f], I.J. Orland[f], K. Kitajima[a,f], J.W. Valley[a,f]

[a] NASA Astrobiology Institute, Department of Geoscience, University of Wisconsin, 1215 W. Dayton St., Madison, WI 53706, USA
[b] Australian Centre for Astrobiology, and School of Biological, Earth and Environmental Sciences, University of New South Wales, Kensington, NSW 2052, Australia
[c] Geological Survey of Western Australia, 100 Plain Street, Perth, WA 6004, Australia
[d] Lamont-Doherty Earth Observatory of Columbia University, 61 Route 9W, Palisades, NY 10964, USA
[e] Curtin University of Technology, GPO Box U1987 Perth, WA 6845, Australia
[f] WiscSIMS, Department of Geoscience, University of Wisconsin, 1215 W. Dayton St., Madison, WI 53706, USA
[g] Fort Lewis College, Department of Geosciences, 1000 Rim Drive, Durango, CO 81301, USA

ARTICLE INFO

Keywords:
Archean
Chert
Oxygen isotopes
Strelley Pool Formation
Secular trends
SIMS
Stromatolite

ABSTRACT

The significance of oxygen isotope ratios in Archean chert has long been debated. Cherts from the c. 3.4 Ga Strelley Pool Formation (SPF) (Pilbara Craton, Western Australia) host some of the oldest stromatolite and microfossil evidence for life, but the genesis and timing of silica cements has been unclear. Field relations, petrography and a combination of laser fluorination and in-situ SIMS measurements of $\delta^{18}O$ in quartz show that bedded cherts of the SPF were originally precipitated as carbonates and were later widely replaced by quartz. Three localities were studied and analyzed for $\delta^{18}O(Qz)$ in chert: 1) Camel Creek: foliated, metamorphosed, bedded cherts and meter-scale black chert veins; 2) Unconformity Ridge and ABDP8 drill core: stromatolitic and bedded chert overlying basal detrital quartz sandstone; and 3) the Trendall locality: "bedded" stromatolitic chert replacing original dolomite, low temperature hydrothermal quartz, and mm- to decimeter-scale chert-quartz veins. Laser fluorination (mm-scale) values of $\delta^{18}O(Qz)$ range from: 14.2 to 18.2‰ VSMOW at Camel Creek; 9.3 to 18.9‰ at Unconformity Ridge; and 13.7 to 25.7‰ at Trendall. Values of $\delta^{18}O(Qz)$ in cm to decimeter-scale hydrothermal chert veins cutting bedded carbonates at Trendall range from ca. 15 to 16‰, whereas "bedded cherts" are 17 to 26‰. These laser data include the highest $\delta^{18}O$ values reported for cherts in Paleoarchean sediments and are up to 4‰ higher than the upper limit of ~22‰ reported in other studies, in apparent contrast to the long-standing secular-temporal trend which shows such high $\delta^{18}O$ only in younger chert. However, analysis by laser fluorination at the 1-mm scale cannot resolve microtextures seen petrographically. In contrast, in-situ SIMS analyses can resolve petrographic microtextures and show $\delta^{18}O(Qz)$ at 10-μm scale have an even greater range of 7–31‰ in "bedded" cherts at the Trendall locality, up to 9‰ above the secular-temporal trend.

Textures observed optically at the Trendall locality were classified as: microquartz, mesoquartz, chalcedony, megaquartz veins, and cavity megaquartz. SEM-CL imaging shows two generations of meso- and megaquartz; bright CL with well-developed growth zoning, and dark CL with massive or mottled texture. Microquartz is the earliest textural generation of quartz and has a maximum $\delta^{18}O(Qz)$ of ~22‰ by SIMS. Dark-CL mesoquartz has similar $\delta^{18}O$ to microquartz and is interpreted to also be early. Bright-zoned-CL mesoquartz, which formed post-Archean, has even higher $\delta^{18}O$, up to 29‰. Vein megaquartz crosscuts most quartz generations and has a restricted range of $\delta^{18}O$, mostly from 16 to 19‰. Chalcedony pseudomorphs rhombic cavities and fractures, lines the edges of veins, and has similar $\delta^{18}O$ to veins (16–19‰). Late cavity megaquartz is bright and zoned by CL, grows into late open cavities, and has the highest $\delta^{18}O(Qz)$ values reported from the Pilbara, up to 31.3‰. Thus, the highest-$\delta^{18}O$ quartz cements at the Trendall locality are the youngest and may be related to weathering. Early silicification and the formation of microquartz, chalcedony and low $\delta^{18}O$ mesoquartz occurred during low temperature hydrothermal activity in the Archean.

None of the SPF quartz examined is interpreted to have formed as a direct precipitate from Paleoarchean seawater. Thus, values of $\delta^{18}O(Qz)$ do not record either water chemistry or temperature of Archean oceans. In-situ SIMS analysis shows that high-$\delta^{18}O(Qz)$ values above 22‰ are only found in late-forming cavity megaquartz and bright-zoned-CL mesoquartz at the Trendall locality.

* Corresponding author at: Fort Lewis College, Department of Geosciences, 1000 Rim Drive, Durango, CO 81301, USA.
E-mail addresses: jncammack@fortlewis.edu (J.N. Cammack), valley@geology.wisc.edu (J.W. Valley).

https://doi.org/10.1016/j.precamres.2017.11.005
Received 14 May 2017; Received in revised form 4 October 2017; Accepted 13 November 2017
Available online 14 November 2017

The SPF results from our sample suite demonstrate the ability to resolve complex history using detailed petrography and SIMS analysis. Similar studies may show equal complexity of $\delta^{18}O(Qz)$ data for other localities that are interpreted to show secular-temporal trends for chert. The apparent increase of $\delta^{18}O(Qz)$ through time may reflect differences in diagenesis, and/or an inherent and previously unrecognized sampling bias that compares fundamentally different populations of quartz, such as Archean hydrothermal chert from volcanic greenstone belts, with unrelated Phanerozoic biogenic quartz.

1. Introduction

Systematically lower oxygen isotope ratios in cherts with increasing age were one of the earliest observations of stable isotope geochemistry (Degens and Epstein, 1962) and have been reinforced by many subsequent studies (Knauth, 1992, 2005; Robert and Chaussidon, 2006; Perry and Lefticariu, 2007; Shields, 2007; Cunningham et al., 2012; Tartèse et al., 2017) (Fig. 1). Similar secular-temporal oxygen isotope trends are observed for carbonates (Perry and Tan, 1972; Veizer and Hoefs, 1976; Veizer et al., 1999; Prokoph et al., 2008) and phosphates (Karhu and Epstein, 1986; Blake et al., 2010). Secular trends in oxygen isotope ratios have led to controversial conclusions that: Archean oceans were warmer (> 60 °C) than Phanerozoic oceans (Karhu and Epstein, 1986; Knauth, 2005; Robert and Chaussidon, 2006; Schwartzman et al., 2007; Tartèse et al., 2017); $\delta^{18}O$ of seawater was lower (Walker and Lohmann, 1989; Kasting et al., 2006; Jaffrés et al., 2007); or older cherts are more altered and do not retain their primary $\delta^{18}O$ (Degens and Epstein, 1962, 1964; Shields, 2007).

Most previous studies analyzed bulk samples at the mm-to-cm scale and were unable to resolve zoning or other petrographically defined variations with correlated oxygen isotope trends at the μm scale. Secondary ion mass spectrometry (SIMS) has allowed in-situ analysis of oxygen isotope ratios in quartz at the 10-μm scale (Hervig, 1992; Valley and Graham, 1996; Kelly et al., 2007; Valley and Kita, 2009). More recently, SIMS has been applied to cherts (Robert and Chaussidon, 2006; Marin et al., 2010; Marin-Carbonne et al., 2014). Low values of $\delta^{18}O(Qz)$ in Fig. 1 are typically interpreted to result from diagenetic alteration and exchange with meteoric or hydrothermal fluids (Perry and Tan, 1972; Knauth, 2005; Robert and Chaussidon, 2006), and elevated $\delta^{18}O(Qz)$ values have been accepted as the 'least altered' chert and most pristine record of seawater by these authors.

This study examines cherts in the ~3.4 Ga Strelley Pool Formation (SPF) of the Pilbara Craton, Western Australia using new SIMS $\delta^{18}O(Qz)$ data correlated to micro-textures in order to address questions of chert genesis and aid in interpreting the secular-temporal trend of $\delta^{18}O$ (Fig. 1). No previous studies of the SPF have combined in-situ SIMS microanalysis of $\delta^{18}O$ with detailed petrography. Values of $\delta^{18}O(Qz)$ from the SPF are used to test three hypotheses that would explain a secular trend: elevated Archean seawater temperatures; changing $\delta^{18}O$ of seawater; or alteration of quartz. This project integrates regional, outcrop and mm- to μm-scale petrographic studies of SPF quartz textures in conjunction with SIMS and laser fluorination (LF) $\delta^{18}O$ measurements on quartz and cherts from bedded, stromatolitic, and detrital lithostratigraphic members of the Strelley Pool Formation (SPF). The $\delta^{18}O(Qz)$ data test petrographic and temporal relations that provide insight into the secular $\delta^{18}O$ trend of cherts. The primary goal is to determine which, if any, SPF quartz generations precipitated in thermal and isotopic equilibrium with Paleoarchean seawater.

1.1. Mechanisms controlling $\delta^{18}O$ of cherts

In this study, the term chert is used broadly to represent rocks that are > 98% monomineralic, chemically precipitated quartz (e.g., Folk, 1980). The $\delta^{18}O$ of quartz in chert is controlled by the temperature at which it precipitates, $\delta^{18}O$ of formation fluid, and any post-crystallization isotopic exchange. In a water-rich system where quartz is at isotopic equilibrium, increased temperature results in a smaller fractionation [$\Delta^{18}O(Qz\text{-}H_2O)$] and lower $\delta^{18}O(Qz)$ (Pollington et al., 2016) (Supplementary Fig. 1). Phanerozoic and modern cherts often form diagenetically during burial. These cherts follow a reaction pathway starting with dissolution-precipitation of biogenic opal-A (siliceous ooze composed of radiolarian, diatoms and sponge spicules) to opal-CT (hydrous silica), and finally form fibrous chalcedony or microcrystalline quartz (Murata and Nakata, 1974; Keene, 1975; Riech and von Rad, 1979; Hein and Yeh, 1983; Williams and Crerar, 1985; Bohrmann et al., 1994; Knauth, 1994). During this sequence, exchange with diagenetic fluids typically causes the final crystalline quartz to have $\delta^{18}O$ values 6–10‰ lower than the original biogenic opal precursors (Knauth and Epstein, 1976; Matheney and Knauth, 1993; Behl and Garrison, 1994). However, if the concentration of silica in diagenetic fluids remains below the solubility of opal-CT (Kastner et al., 1977; Siever, 1992), then chert may form directly from opal-A.

1.2. The secular-temporal trend of $\delta^{18}O$ chert

Archean to Mesoproterozoic chert is inherently different from Phanerozoic cherts. There was no known biogenic silica fixation by organisms prior to the evolution of Ediacaran sponges at c. 543–549 Ma (Brasier et al., 1997; Wang et al., 2010). In the absence of biogenic silica fixation, marine silica concentrations may have exceeded 60 ppm (Siever, 1992), with the possibility of abiogenic silica precipitation under ambient seawater temperatures (Knauth, 1994; Gunnarsson and Arnórsson, 2000; Perry and Lefticariu, 2007).

Fig. 1 shows the compiled values for $\delta^{18}O(Qz)$ in Precambrian to

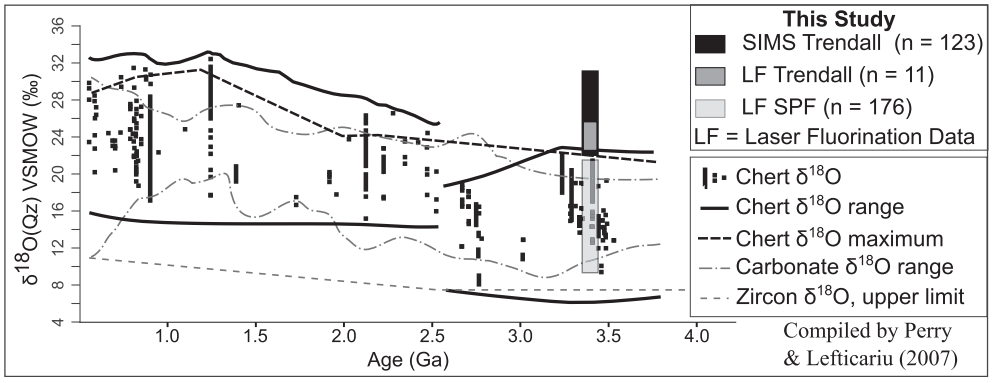

Fig. 1. Chert $\delta^{18}O$ secular-temporal trend through time. Data ranges from this study are shown at 3.4 Ga. Ages shown on this figure represent the depositional ages for the samples shown, and do not reflect the ages of alteration events affecting these cherts (see text). LF indicates bulk mm-sized laser-fluorination $\delta^{18}O$ analyses. The SIMS data represent measured cherts from the Trendall Locality that have elevated $\delta^{18}O$. Figure modified from Perry and Lefticariu (2007): $\delta^{18}O$ data and range for cherts (Knauth, 2005), chert $\delta^{18}O$ maximum (Robert and Chaussidon, 2006), carbonate $\delta^{18}O$ range (Shields and Veizer, 2002), zircon $\delta^{18}O$ upper limit (Valley et al., 2005).

Phanerozoic chert (from Perry and Lefticariu, 2007). Cherts found in units of older depositional-age are lower in $\delta^{18}O$ and there is an apparent step up to higher values at the end of the Archean. Solid lines define the range of $\delta^{18}O$(Qz). The black-dashed line represents the maximum chert $\delta^{18}O$ from Robert and Chaussidon (2006) and the grey dot-dash lines represent the range of carbonate $\delta^{18}O$ from Shields and Veizer (2002).

1.2.1. Ocean temperature in the Archean

Many studies have interpreted chert $\delta^{18}O$ data as a paleoclimate proxy and estimated seawater temperatures in excess of 60 °C during the Archean (Knauth and Lowe, 2003; Knauth, 2005; Robert and Chaussidon, 2006; Schwartzman et al., 2007; Tartèse et al., 2017). Temperature estimates assume that seawater $\delta^{18}O$ has remained relatively constant (ca. 0 ± 1‰) throughout Earth's history, that quartz in chert is unaltered, and that processes of chert formation are comparable to modern environments. Knauth and Lowe (2003) report bulk $\delta^{18}O$ (chert) data uniformly below 22‰ in 3.5 Ga metamorphosed bedded cherts from the Barberton Greenstone Belt in South Africa. They discussed a possible 6–10‰ reduction in $\delta^{18}O$ during diagenesis from opal to chert, but interpreted the highest $\delta^{18}O$(Qz) values as a paleotemperature proxy for Archean seawater, reasoning that some cherts that originally had $\delta^{18}O$ values above 22‰ were lowered in $\delta^{18}O$ by diagenesis. Karhu and Epstein (1986) analyzed $\delta^{18}O$ in phosphates that were interpreted to be co-precipitated with quartz in cherts and estimated seawater temperatures as high as 80 °C. If waters are assumed to be marine, these results are interpreted to indicate little change in $\delta^{18}O$ (seawater).

There are several lines of evidence that argue against uniformly hot Archean oceans. The upper temperature limit for chlorophototrophy is ~73 °C (Brock and Brock, 1968; Boyd et al., 2010; Hamilton et al., 2012). If organisms responsible for forming stromatolites in the Archean and Paleoproterozoic included chlorophotoautrophs, which seems likely given their conical morphology and photic zone sedimentary facies (Hofmann et al., 1999; Allwood et al., 2007), temperatures should have been 60 °C or less for these organisms to thrive (Hamilton et al., 2012). The Archean sun was ~70% as luminous as today, leading some to conclude that the Earth's oceans would have frozen in the absence of a very thick greenhouse atmosphere (Sagan and Mullen, 1972; Kasting, 1993). Glacial diamictites at ~2.9 Ga in the Kaapvaal Craton of South Africa (Young et al., 1998) were deposited at an estimated paleolatitude of 48° (Nhleko, 2003) and low paleolatitude (4–11°) glacial diamictite deposited at ~2.4–2.3 Ga in the Huronian Supergroup of Ontario (Williams and Schmidt, 1997) further argue against uniformly hotter Precambrian oceans. Blake et al. (2010) measured $\delta^{18}O$ of 16–20‰ for Paleoarchean phosphates and estimated temperatures from 26 to 35 °C in surface seawater (assuming $\delta^{18}O$ (water) = 0‰).

1.2.2. Seawater $\delta^{18}O$ in the Archean

Changes in the $\delta^{18}O$ of seawater are likewise controversial. Values of $\delta^{18}O$(seawater) as low as −12 ‰ VSMOW have been proposed for the Precambrian (Jaffrés et al., 2007). In contrast, modern seawater $\delta^{18}O$ is relatively consistent at ~0 ± 1‰ (Hoefs, 2015). Small, short-term changes in seawater $\delta^{18}O$ are caused by variations in the amount of meteoric water stored on the continents as ice during glacial (seawater $\delta^{18}O \approx +1$‰) or inter-glacial (≈ -1‰) periods (Jaffrés et al., 2007; Perry and Lefticariu, 2007). Seawater $\delta^{18}O$ might also vary due to changes in global water-rock interaction such as hydrothermal activity at mid-ocean ridges, which vary with seafloor spreading rates. Tartèse et al. (2017) measured $\delta^{18}O$ in organic matter from Precambrian cherts and concluded that $\delta^{18}O$(seawater) was 0 ± 5‰ throughout the Archean.

Rock altered by hydrothermal activity at mid-ocean ridges provides another line of evidence for seawater $\delta^{18}O$ trends. The modern $\delta^{18}O$ value of seawater (0‰) results from an average $\delta^{18}O$ of altered oceanic crust (~6‰) and an average $\Delta^{18}O$(rock-seawater) ~6‰ (Gregory, 1991). If seawater changed in $\delta^{18}O$, then the $\delta^{18}O$ of altered rocks would be affected. However, $\delta^{18}O$ values of Archean pillow basalts from the Pilbara (~6–12‰, Gregory, 1991) are similar to those in Cenozoic ophiolites (Muehlenbachs, 1998). Based on mass-balance models, Gregory (1991) estimated that seawater remained at −1.3 ± 1‰ and Muehlenbachs (1998) estimated 0 ± 2‰ throughout Earth's plate tectonic history. Putative Archean eclogite with $\delta^{18}O$ values of 4.7–6.9‰ (Jacob, 2004) suggest subduction of oceanic basalt altered by seawater similar to today as early as 3 Ga (Jacob et al., 1994; Jacob, 2004; Shirey and Richardson, 2011).

1.2.3. Alteration of Archean chert

It has also been proposed that older rocks (cherts, carbonates and phosphates) are more altered on average and thus have lower $\delta^{18}O$ (Degens and Epstein, 1962, 1964; Karhu and Epstein, 1986; Shields, 2007; Prokoph et al., 2008). However, the proposal that low $\delta^{18}O$ Archean cherts result largely from alteration has been challenged on the basis that carbonates would be more strongly affected by alteration than cherts and that phosphates would be less altered. Thus, these rocks/minerals should not have the similar ~10‰ secular trends that cherts show (Wenzel et al., 2000; Kasting et al., 2006).

In summary, none of these three interpretations adequately explains the secular trend of $\delta^{18}O$(Qz) for cherts.

2. Geology of the Strelley Pool Formation

The Strelley Pool Formation (SPF) sedimentary rocks are a prominent regional stratigraphic marker that is recognized in 11 of the 20 greenstone belts throughout the East Pilbara Terrane in Western Australia (Fig. 2) (Hickman, 2008). The SPF unconformably overlies the Warrawoona Group (Buick et al., 1995; Van Kranendonk, 2006) and conformably underlies the 3350 Ma Euro Basalt of the Kelly Group (Hickman, 2008; Wacey et al., 2010). Conglomerates and sandstones of variable thickness mark the unconformity at the base of the SPF, which locally is subaerial and represents the oldest known angular unconformity on Earth (Buick et al., 1995). Breccias and conglomerates at the top of the SPF, derived from lower SPF members, indicate a second period of erosion prior to the deposition of the Euro Basalt (Hickman, 2008). Based on zircon geochronology from the Warrawoona (3530–3427 Ma) and Kelly (3350–3315 Ma) Groups, SPF deposition occurred after 3427 Ma and ceased before 3350 Ma (Nelson, 1998; Van Kranendonk et al., 2002; Van Kranendonk and Pirajno, 2004; Hickman, 2008; Wacey et al., 2010). SPF deposition thus represents a volcanically quiescent period of up to 75 Myr (Hickman, 2008).

The Strelley Pool Formation includes some of the oldest, low-grade cherts and offers unique opportunities to evaluate conditions on the early Earth. The first detailed study of the Strelley Pool Formation by Lowe (1983) interpreted portions of the SPF as silicified carbonate and evaporite deposits from a peritidal, partially-restricted marine environment and numerous studies have corroborated these interpretations. The SPF hosts unsilicified, partially-silicified, and completely silicified dolomitic stromatolites comprising spectacular macroscopic evidence for early life on Earth (Hofmann et al., 1999; Allwood et al., 2007). Several studies provide morphological and geochemical evidence for microfossils and biogenic kerogen preserved in microcrystalline quartz of the SPF (Wacey et al., 2011a; Lepot et al., 2013; Sugitani et al., 2013; Brasier et al., 2015; Duda et al., 2016). These structures are now generally accepted as strong evidence for life at ~3.4 Ga, although the stromatolitic forms were once interpreted as abiogenic (Lowe, 1994; Lindsay et al., 2005).

2.1. Strelley Pool Fm. lithostratigraphy and sample localities

The SPF consists of three major lithostratigraphic members (Van Kranendonk, 2011). Member 1 (M1) at the base is composed of coarse

to medium-grained clastic units of sandstone and pebble to boulder conglomerate. Member 2 (M2) has bedded dolomite, stromatolitic dolomite, radiating crystal fans replaced by dolomite and largely silicified, and partly to completely silicified stromatolitic dolomite. Member 3 (M3) at the top is a coarse clastic unit chiefly composed of cobble to boulder conglomerates, coarse sandstones, and breccia. Anastomosing, decimeter- to meter-scale, grey to black hydrothermal veins that are primarily composed of black, very fine-grained quartz (chert) that cut across and parallel to bedding in all three members (Van Kranendonk, 2011:Fig. 3 and Supplementary Fig. 2). Veins are locally observed in the underlying Warrawoona Group and terminate within the SPF; veins do not cross up into the Euro Basalt overlying the SPF (Van Kranendonk et al., 2001; Van Kranendonk and Pirajno, 2004; Van Kranendonk, 2011). Smaller quartz veins (mm- to-μm scale) are observed in thin section to cut across chert textures.

2.1.1. Trendall locality

The majority of SIMS $\delta^{18}O$ data in this study are from M2 of the Strelley Pool Formation, collected from the Trendall locality (Figs. 2 and 3). This area (the Trendall Reserve) has been protected from

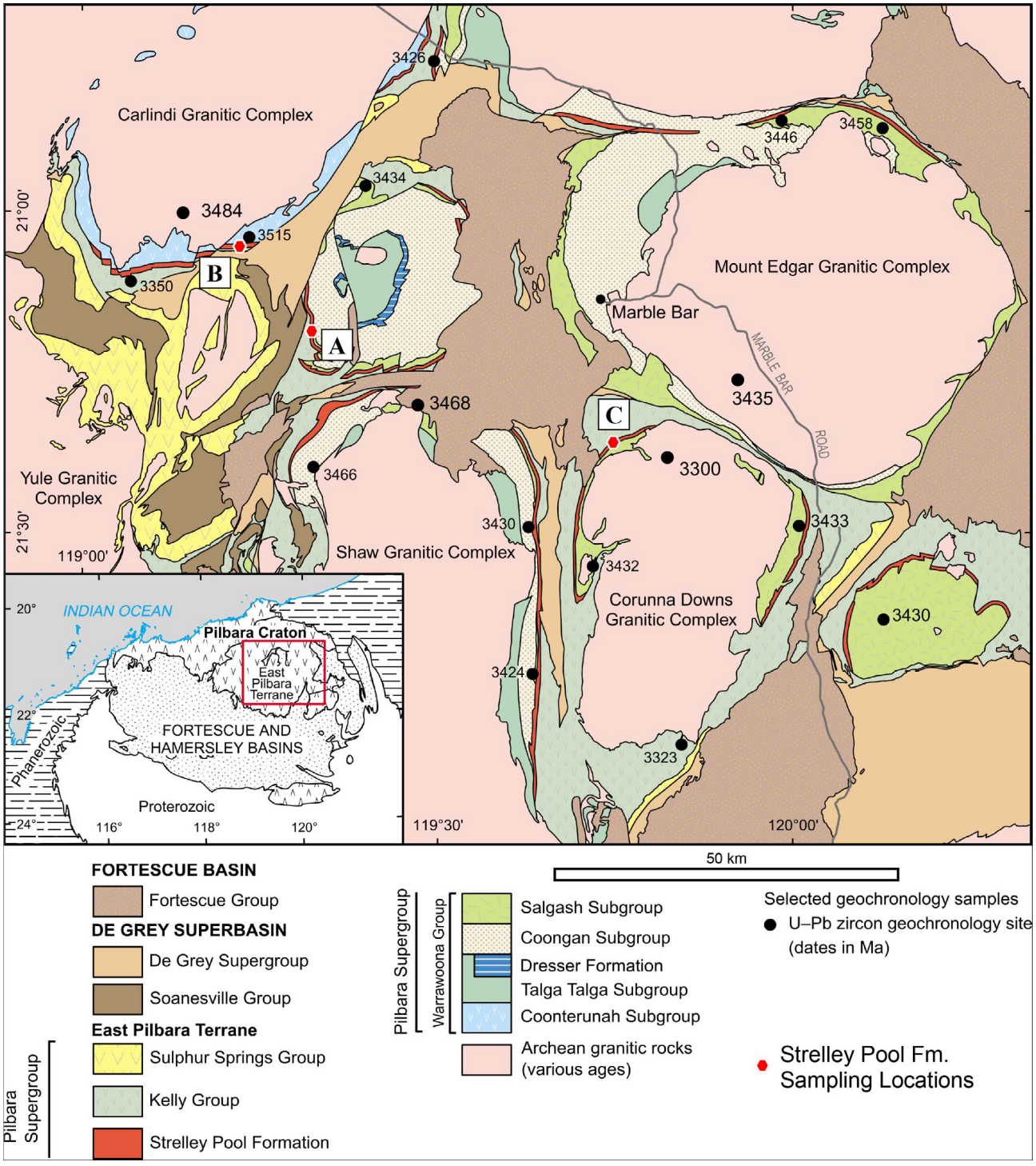

Fig. 2. Simplified geologic map of the East Pilbara Terrane of the Pilbara Craton, Western Australia, showing the Strelley Pool Formation sampling locations. A – Trendall Locality. B – Unconformity Ridge. C – Camel Creek. Base-map is from Hickman (2008).

unauthorized sampling since 2009 because it includes exceptional examples of coniform stromatolitic dolomite and chert (Hofmann et al., 1999; Hickman et al., 2011; Van Kranendonk, 2011). Samples analyzed here were collected from float prior to 2009.

The SPF at the Trendall locality is cut by decimeter- to meter wide, dark grey to black hydrothermal chert veins, which were analyzed for $\delta^{18}O$(Qz) and compared to the M2 "bedded" cherts (silicified bedded dolomites: Fig. 3 and Supplementary Fig. 2). Data and interpretations from the Camel Creek locality and from the Unconformity Ridge locality are also reported for comparison to the Trendall locality, based on details presented in Cammack, 2015.

2.2. Post-depositional and penecontemporaneous processes

In this study, 'hydrothermal' is used broadly to describe circulating fluids that were warmer (i.e., 50–350 °C) than the rocks they interacted with. Many studies have documented geochemical and field evidence of hydrothermal activity and silicification in the SPF and other units of the Pilbara Supergroup (Buick et al., 1981; Lowe, 1983; Buick and Dunlop, 1990; Van Kranendonk et al., 2003; Van Kranendonk and Pirajno, 2004; Sugitani et al., 2006; Van Kranendonk, 2006; Hickman, 2008; Rouchon and Orberger, 2008; Wacey et al., 2010; Boorn et al., 2007, 2010).

Member 2 of the SPF at the Trendall locality contains bedded and stromatolitic dolomite with molar Fe/(Mg + Fe) = 0–0.1 (Appendix 2 and Supplementary Table 7 in Cammack, 2015). These rocks are partially-silicified and can be seen to grade into adjacent fully-silicified counterparts (Van Kranendonk, 2011: Supplementary Fig. 2 A-E). The fully silicified stromatolitic samples contain mm- to μm-scale rhombic cavities, some with dolomite rhombs and some with chalcedony pseudomorphs (Supplementary Fig. 3 E, F).

Hydrothermal chert veins cut across the bedded SPF rocks and branch into smaller quartz veins that have silicified the adjacent carbonates to form what appear as "bedded" cherts (Fig. 3 and Supplementary Fig. 2). In thin-section and by backscattered electron imaging (BSE) on a scanning electron microscope (SEM), the bedded dolomites are coarse and re-crystallized into 200–700 μm crystals. Locally, ferroan dolomite zonation occurs at contacts with quartz veins (Appendix 2 in Cammack, 2015). Despite re-crystallization, dolomites have LREE depletion, elevated Y/Ho and positive La, Gd and Er anomalies relative to chondrites that suggest dolomite precursors precipitated from Archean seawater (Table 1, Figs. 9b, c and 10 of Van Kranendonk et al., 2003).

Van Kranendonk and Pirajno (2004) analyzed the geochemistry and field relations of the Euro Basalt above the Strelley Pool Formation and volcanic rocks immediately beneath the SPF. They noted that hydrothermal alteration of the overlying Euro Basalt was low to absent. However, lenses in the Warrawoona Group immediately beneath the SPF are depleted in CaO and Na_2O and have slight enrichments of K_2O and Al_2O_3, as well as HREE-depleted geochemical patterns. They interpreted these trends as argillic and phyllic alteration by hydrothermal fluids that may have been responsible for some of the silicification in the Strelley Pool Formation. Hydrothermal pyrophyllite and phyllic alteration has also been detected by short wave infrared spectroscopy directly beneath the SPF at the Trendall Locality (Brown et al., 2004, 2006).

Boorn et al. (2007, 2010) analyzed $\delta^{30}Si$ and trace elements in Pilbara Kitty's Gap Chert. Based on differing trends of $\delta^{30}Si$ versus Al_2O_3, they interpreted some cherts as volcanogenic sediments that have been silicified by hydrothermal activity, and others as seawater-precipitated with low volcanogenic input.

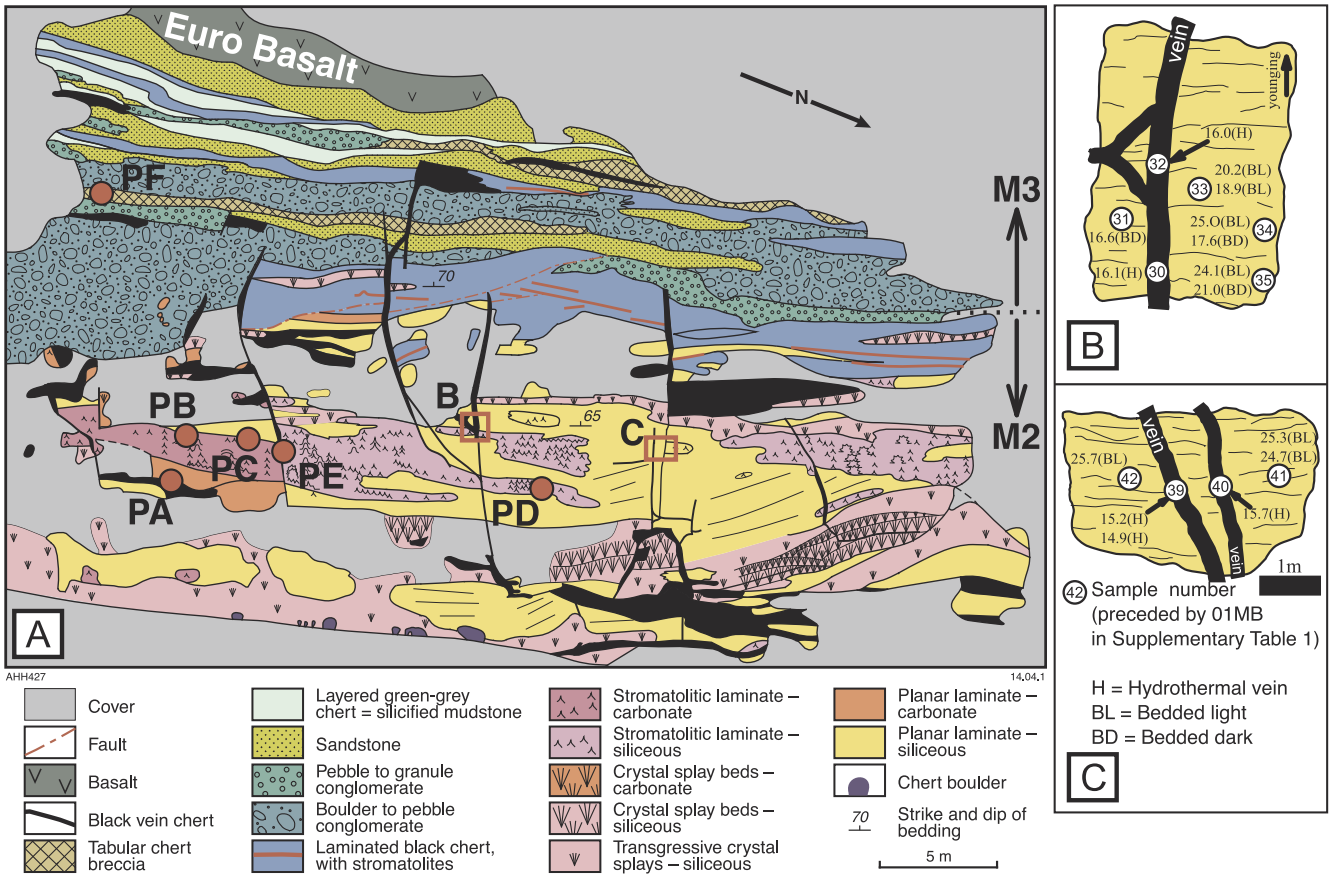

Fig. 3. A – Outcrop map of the Trendall Locality (from Van Kranendonk, 2011). The contact of bedded and stromatolitic M2 to overlying M3 detrital units is indicated. Red points labeled 'PA' to 'PF' correspond to outcrop photos in Supplementary Fig. 2. Locations of parts 'B' and 'C' outlined in red boxes. B and C show detailed sampling locations (Sample numbers in white circles are preceded by 01 MB in Supplementary data tables; e.g. 41 = 01 MB41) with their corresponding average laser fluorination $\delta^{18}O$(Qz) values.

All of the cross-cutting veins observed in this study terminate within the SPF (Fig. 3), indicating that hydrothermal alteration occurred prior to the deposition of the Euro Basalt and may have been synchronous with deposition of the SPF (see also Sugitani et al., 2015).

2.2.1. Metamorphism

Metamorphism and hydrothermal alteration in East Pilbara terrane greenstones is locally variable. Metamorphic grade is generally low (prehnite-pumpellyite to lower greenschist facies), but increases to lower amphibolite facies at contacts of granitoid bodies (hornblende-plagioclase, with local actinolite-garnet). Cummingtonite-grunerite amphiboles in cherts at Camel Creek (Supplementary Fig. 4) indicate contact metamorphism adjacent to the Corunna Downs granitic complex (Cammack, 2015). More generally, the Strelley Pool Formation is typically reported to have experienced lower- to sub-greenschist facies regional metamorphism (Van Kranendonk, 2000; Van Kranendonk and Hickman, 2000; Terabayashi et al., 2003; Van Kranendonk and Pirajno, 2004; Lindsay et al., 2005; Brasier et al., 2006; Wacey et al., 2010).

Microquartz and chalcedony are present in cherts at the Trendall locality. These cements would have re-crystallized to polygonal megaquartz or undulatory megaquartz if heated to greenschist facies regional metamorphism. Likewise, the presence of grains sutured by pressure-solution, syntaxial quartz-overgrowths, and microquartz sandstone cements found at Unconformity Ridge (Valley et al., 2015; Cammack, 2015) would likely have re-crystallized to coarse or polygonal quartz during greenschist-facies metamorphism (Summer and Ayalon, 1995; Holness and Watt, 2001).

2.2.2. Thermal maturity of organic matter in the SPF

Raman spectra for carbonaceous matter provides an index of temperature, but are influenced by other factors including time, deformation and fluids (e.g., Wopenka and Pasteris, 1993; Jehlička et al., 2003). Organic matter in the M1 basal sandstone of the SPF at Unconformity Ridge has Raman spectra interpreted to record lower greenschist facies metamorphism (Wacey et al., 2011b). Organic matter in cherts sampled near the Trendall locality were also interpreted to record lower greenschist facies, with temperatures below 350 °C (Sugitani et al., 2013). However, Allwood et al. (2006b) found that temperatures estimated from organic matter in dolomite varies within a vertical transect of the SPF. They proposed that the stromatolitic M2 unit experienced temperatures less than 200 °C at Trendall, in contrast to adjacent samples of more permeable M1 and M3 that experienced up to ~400 °C. The variable temperature estimates from Raman indicate that the SPF has not uniformly experienced greenschist facies metamorphism and was heated locally by fluid advection (see also Van Kranendonk, 2006 and Terabayashi et al., 2003). The distinction of hydrothermal alteration vs. regional metamorphism is important and suggests that the unusual degree of preservation at the Trendall locality resulted because it escaped intense alteration and was only minimally affected by regional metamorphism.

2.2.3. Weathering and silcretes

At the Trendall locality, dolomitic stromatolites of the Strelley Pool Formation are found near the base of a high chert ridge, along the banks of the Shaw River, which exposed fresher rocks. Stromatolites on ridge-crests across the whole of the East Pilbara Terrane are more completely silicified than in low-lying dolomitic outcrops near riverbanks, suggesting that some silicification at the Trendall locality and elsewhere may be related to weathering (Van Kranendonk, 2000; Hickman, 2008). Cenozoic weathering in the Pilbara region has been documented across Western Australia (Hocking and Cockbain, 1990). Li et al. (2012) found that U enrichment in the Apex Basalt is positively correlated with Fe^{3+}/Fe and occurred in the last 200 Myr as a result of oxidative weathering and meteoric water infiltration. Likewise, $^{40}Ar/^{39}Ar$ geochronology shows that K-Mn oxides from the Pilbara formed episodically as a result of Paleocene weathering (Dammer et al., 1999). These Cenozoic events may have been responsible for at least some of the silicification of the SPF.

3. Methods

3.1. Samples

Samples were collected and drilled in the lab with a 3-mm diamond coring bit and analyzed for $\delta^{18}O$ by laser fluorination (LF). Six Trendall locality samples were selected for more detailed in-situ analysis of $\delta^{18}O$ by SIMS. Sample information is in Supplementary Table 1. Sample locations, photographs and sketches of the Trendall locality can be found in Fig. 3 and Supplementary Fig. 2.

3.2. Microscopy

Each sample was examined by optical and scanning electron microscopy (SEM). Three to seven areas of interest for SIMS analysis (measuring ~500 by 350 μm) were selected in each sample based on examination of the different quartz textures. Optical images in plain and cross-polarized light (XPL) were made of each analysis area and SEM images were taken in backscattered electron (BSE) and cathodoluminescence (CL) modes using a Hitachi S3400 SEM at the Department of Geoscience, UW-Madison (Appendix 6 in Cammack, 2015). Unknown minerals were identified using energy dispersive X-ray spectrometry (EDS) on the SEM. In-situ spot analyses for chemical composition (EPMA), isotope ratios (SIMS), and corresponding imagery of analysis areas (SEM and petrographic microscope) have been managed using Quantum Geographic Information System (QGIS Development Team, 2014) (Appendix 3 in Cammack, 2015).

3.3. Oxygen isotope analysis

All $\delta^{18}O$ values are reported in standard permil (‰) notation relative to the Vienna Standard Mean Ocean Water Standard (VSMOW) (Baertschi, 1976; Coplen, 1988):

$$\delta^{18}O(\text{sample})\ (\text{‰,VSMOW}) = 1000*([^{18}O/^{16}O]_{\text{sample}}/[^{18}O/^{16}O]_{\text{VSMOW}}-1)$$

3.3.1. Laser fluorination & gas-source mass spectrometry (LF)

Samples were analyzed by laser fluorination and gas-source mass spectrometry (LF) at the Stable Isotope Laboratory, Department of Geoscience, UW-Madison. Preliminary selection was based on hand-sample observations of textural differences using a stereoscopic microscope. Samples for LF were treated as needed to remove or aid in the identification of impurities (identified by microscopy) for 5–60 min with 15 M HNO_3 (sulfides), 28 M HF (silicates) and/or 12 M HCl (carbonates). The HF treatment of quartz was used when other silicates were identified; HF was not intended to fully dissolve non-quartz silicates but to partially react, making them easier to avoid during preparation of splits for LF. Partial dissolution has no effect on $\delta^{18}O$ of residual quartz grains (Kelly et al., 2007). Final quartz separates were > 99% pure. Purified quartz splits weighing 1–2 mg were individually loaded along with aliquots of UWG-2 garnet standard into a 70-sample nickel plug for LF analysis.

Bulk quartz samples were converted to CO_2 using laser-heating and fluorination with the rapid-heating, defocused-beam technique. CO_2 was analyzed by Finnigan/MAT 251 triple-collecting gas-source mass-spectrometer (Valley et al., 1995; Spicuzza et al., 1998). Samples by LF were standardized with UWG-2 garnet standard ($\delta^{18}O$ = 5.80‰, Valley et al., 1995). External precision based on multiple analyses of UWG-2 on each day of analysis average ± 0.10‰ (2SD) for all LF measurements reported here (Supplementary Table 2).

3.3.2. Secondary ion mass spectrometry (SIMS)

SIMS analyses were made using a CAMECA IMS-1280. Procedures have been reported previously (Kelly et al., 2007; Kita et al., 2009; Valley and Kita, 2009); a brief description follows. Samples were mounted within 5 mm of the center of 25-mm diameter round samples and polished to a low-relief surface (Kita et al., 2009). One to two grains of UWQ-1 quartz standard ($\delta^{18}O = 12.33‰$, Kelly et al., 2007) were cast near the center of each sample. An electron flood gun was used to aid charge neutralization at the C-coated sample surface. A $^{133}Cs^+$ beam with a sample current of ~2 nA was accelerated at 10 keV (impact energy = 20 keV) and focused on the sample surface to a diameter of ~10 μm (~1 μm deep) for each pit. Secondary O^- ions were accelerated at −10 kV into a double-focusing, large-radius mass spectrometer where $^{16}O^-$ and $^{18}O^-$ ions were collected by two Faraday Cup detectors. A third Faraday Cup measured $^{16}O^1H$, which was resolved from ^{17}O. The average ratio of $^{16}O^1H/^{16}O$ from each UWQ-1 bracket was subtracted from each sample measurement to obtain background-corrected $^{16}O^1H/^{16}O$ values (Wang et al., 2014), that are used to monitor contamination and the possible presence of hydrous silica. Pits were pre-sputtered with the Cs beam for ~10 s prior to an automated routine that centered the secondary ion beam in the field aperture. For each pit, counting and integration was conducted for 80 s (20 cycles of 4 s /ea.).

For each SIMS session, sample analyses were standardized every 5–17 measurements by bracketing with 8–12 spots on the UWQ-1 quartz standard. Spot-to-spot external repeatability of UWQ-1 averaged 0.24‰ 2SD and was at or below 0.5‰, 2SD for all reported data. SIMS $\delta^{18}O$ data are reported in Supplementary Table 3. After analysis, pits were imaged by SEM and petrographic microscope to verify the mineral texture that was analyzed and to exclude analyses that hit other phases or contaminants such as epoxy.

4. Results

4.1. Mineralogy

Most thin sections presented here are nearly 100% quartz. In some bedded M2 cherts from the Trendall locality, samples contained minor dolomite, siderite or late calcite veins and trace sulfides (Kozdon et al., 2010), apatite, barite, sericite, and Fe-Mn oxides. Partly silicified stromatolitic dolomites were also examined from Trendall that are composed of 0–50% quartz and 50 to > 90% dolomite (Cammack, 2015).

4.2. Quartz textures and petrology

Several textures of quartz were identified using plain light (PL), cross-polarized light (XPL), and cathodoluminescence (CL) by SEM. Representative photomicrographs of quartz textures are shown in Fig. 4 with corresponding XPL and CL images, showing SIMS analysis spots and values of $\delta^{18}O$(Qz). Appendix 6 in Cammack (2015) has BSE, CL and XPL imagery of every SIMS analysis area and corresponding $\delta^{18}O$ (Qz) values.

4.2.1. Trendall locality textures

The textural definitions of microquartz, mesoquartz, and megaquartz described below are based on Folk and Weaver (1952) and Maliva et al. (2005). The textures and their relative timing at the Trendall locality were determined by optical and SEM petrography, and are listed in Table 1 and depicted in Fig. 4.

Microquartz is commonly less than 10 μm in diameter. Mesoquartz has crystals from 20 to 50 μm. Microquartz and mesoquartz both have crenulated crystal boundaries and diffuse extinction in XPL. They are often associated with rhombohedral cavities, rhombohedral chalcedony pseudomorphs and occasional 2–200 μm dolomite crystals that are surrounded by either microquartz or mesoquartz (Supplementary Fig. 3). Microquartz and mesoquartz typically exhibit dark or mottled CL textures (Fig. 4A and B).

Megaquartz from the Trendall locality is greater than 50 μm in diameter with planar crystalline boundaries and sharp, non-undulose extinction in XPL. Megaquartz is divided into two categories: vein megaquartz and cavity megaquartz. It was not always possible to distinguish cavity vs. vein megaquartz in a 2D thin section. Megaquartz which was not distinguishable as vein megaquartz or cavity megaquartz was categorized as 'megaquartz' without a modifier (Fig. 4C).

Vein megaquartz in 100 to 1000-μm wide veins is observed to cut all other textural varieties with the exception of cavity megaquartz at the Trendall locality (Supplementary Fig. 5). It often surrounds 1–20 μm dolomite crystals (Supplementary Fig. 3D) (identified using EDS) and occasionally contains ~1–3-μm, aqueous, fluid-vapor inclusions. It tends to be dark and massive or mottled in CL (Supplementary Fig. 5).

Cavity megaquartz was only observed at the Trendall locality in M2.

Table 1
Quartz textures and relative timing for cementation in chert of the Strelley Pool Formation at the Trendall Locality.

Texture	Relative Timing	Petrographic relations and Observations	Formation Hypotheses, Interpretations
Microquartz	1a	< 20 μm crystals, crenulated boundaries, diffuse extinction in XPL. Contains rhombohedral cavities surrounded by cavity megaquartz, local 1–200 μm dolomite. Cut by vein megaquartz, mesoquartz, and chalcedony. Dark-mottled CL.	First quartz generation. Replaces carbonate. Silicifying fluids supplied by decimeter-meter scale feeder veins infiltrating M2.
Mesoquartz (dark CL)	1b	> 20 μm crystals, crenulated boundaries. Often adjacent to microquartz. Contains rhombohedral-cavities, Local 1–200 μm dolomite. Cut by vein megaquartz. Dark-mottled CL.	Forms by hydrothermal fluid-microquartz interaction. This results in nucleation on and coarsening of microquartz during one or more silicification events with similar $\delta^{18}O$(fluid) and temperatures.
Chalcedony	1c	Forms at the edges of megaquartz veins. Also fills cavities. May form rhombohedral carbonate pseudomorphs in microquartz and mesoquartz. Length fast and slow varieties. Dark-mottled CL.	Similar $\delta^{18}O$(Qz) & petrographic relationships suggests a relationship with hydrothermal veins.
Megaquartz Veins	1d	> 50 μm crystals with planar boundaries and unit extinction. Crosscuts all other generations except cavity megaquartz. Occurs both as cm-m scale veins and mm-μm scale veins. Dark-mottled CL.	Fluid conduits replacing SPF carbonate protolith by hydrothermal fluids infiltrating and bifurcating into M2 bedded carbonates. $\delta^{18}O$ difference in outcrop scale vs. mm veins due to: cooling fluids, $\delta^{18}O$ fluid-carbonate exchange or different veining events.
Mesoquartz (bright-zoned-CL)	2a	Associated with cavity megaquartz and often near the roots of the euhedral drusy crystals. Often bright in CL and zoned similar to cavity megaquartz. Not crosscut by veins.	Late nucleation & $\delta^{18}O$ exchange on microquartz. Related to cavity megaquartz formation event.
Cavity Megaquartz	2b	Found in < mm cavities. Euhedral drusy quartz crystal growths point into cavities. Not crosscut by veins. Bright and zoned in CL.	Late quartz cements likely related to weathering.

Abbreviations: XPL = crossed polarized light microscopy; CL = cathodoluminescence imaging; M1, M2 = SPF members 1, 2.

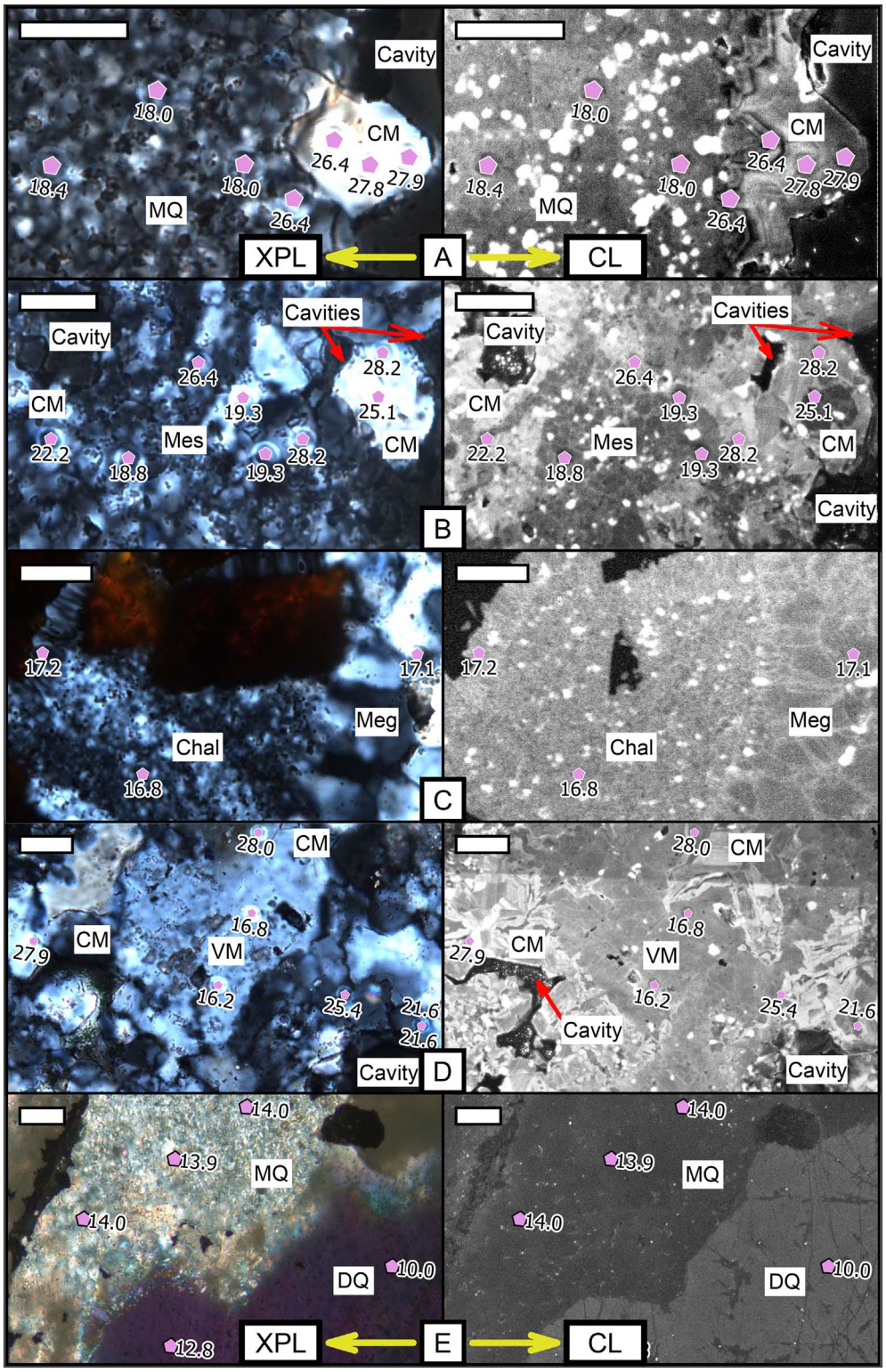

Fig. 4. Strelley Pool Formation quartz textures with SIMS $\delta^{18}O$ analyses in matching XPL (Cross-polarized light optical microscopy) and CL (Cathodoluminescence) images. All scale bars = 50 µm. A to D are samples from the Trendall Locality. E is from Unconformity Ridge. A – microquartz and cavity megaquartz (sample 01MB41A). B – cavity megaquartz and mesoquartz (sample 01MB41B). C – chalcedony and megaquartz (sample 01MB42B). D – cavity megaquartz and vein megaquartz (sample 01MB42A). E – Sandstone, thin section is ~100 µm thick (sample 12-ABDP8@151.83). Abbreviations are: Chal = chalcedony, CM = cavity megaquartz, DQ = detrital quartz, MQ = microquartz, Mes = mesoquartz, Meg = megaquartz, VM = vein megaquartz. Bright white spots in CL images are from residual alumina polishing grit.

It is often drusy with euhedral crystal terminations that surround and point into the center of 50–250 µm rock cavities (Fig. 5A). These rock cavities are occasionally rhombohedral (Supplementary Fig. 3B and E). Oscillatory growth zoning is commonly seen in CL images of cavity megaquartz (Fig. 5B). Some mesoquartz, commonly found near the basal sections of drusy cavity megaquartz, is distinctly bright and sometimes zoned when imaged with CL (Fig. 4B).

Chalcedony from the Trendall locality occurs as radiating, fibrous, cavity filling cements and sandstone cements in M2 It is also found with vein megaquartz occurring near the contacts of the vein with the surrounding matrix. Occasionally it occurs as rhombohedral shapes (Supplementary Fig. 3F). Chalcedony occurs throughout the SPF samples of this study as both length fast and length slow varieties. Chalcedony often exhibits dark, fibrous or mottled CL textures similar to microquartz (Fig. 4C).

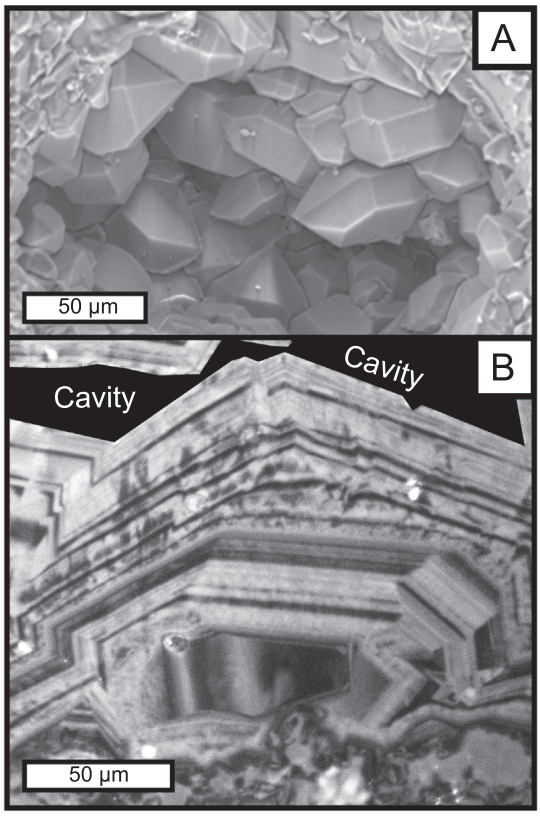

Fig. 5. A – Scanning Electron Microscope image of cavity megaquartz from the Trendall locality (sample 01 MB41). B – Cathodoluminescence image with zoned "cavity megaquartz" from the Trendall locality (sample 01 MB33). The cavity has been colored black.

4.3. Laser fluorination oxygen isotope analyses (mm-scale)

Laser Fluorination (LF) measurements at mm-scale were conducted to regionally survey the $\delta^{18}O(Qz)$ of SPF cherts (Fig. 6, Supplementary Table 2). Camel Creek has $\delta^{18}O(Qz)$ values that average 15.7‰, and show a relatively small range from 14.2 to 18.2‰ for 17 samples collected up to 400 m apart (Supplementary Table 2). Unconformity Ridge samples have an average $\delta^{18}O(Qz)_{LF}$ = 13.6 and range from 9.3 to 18.9‰. The Trendall locality (SPF) has significantly higher $\delta^{18}O(Qz)_{LF}$ values ranging from 13.7 to 25.7‰. Decimeter- to meter-scale hydrothermal veins at Trendall that cut chert bedding have average $\delta^{18}O(Qz)_{LF}$ = 15.6, and range from 14.9 to 16.1‰.

4.4. SIMS oxygen isotope analyses (µm-scale)

Based on laser fluorination analyses, nine samples were selected for in-situ SIMS analysis (Fig. 7). Six samples were from the Trendall locality, one from Camel Creek and two from Unconformity Ridge (Supplementary Table 1). Texturally homogenous foliated polygonal quartz (50–200 µm) in one sample from Camel Creek has low variability $\delta^{18}O(Qz)$ (average = 15.5 ± 0.3‰, 2SD, N = 17). Analysis of two samples from outcrop on Unconformity Ridge, from near the stratigraphic top and bottom of M1, show that sandstone cements are also homogenous in $\delta^{18}O$ (ave. = 13.9 ± 0.4‰ 2SD, N = 50). Detrital quartz $\delta^{18}O$ values are 10.0–13.8‰ and average 12.6‰ at Unconformity Ridge (Fig. 7A). The Trendall locality samples show an even greater, 24‰ range in $\delta^{18}O(Qz)$ (7.3–31.3‰, N = 252).

The SIMS $\delta^{18}O$ values of the different quartz textures are plotted as histograms for each sample location in Fig. 7. Megaquartz and mesoquartz from Trendall have bimodal $\delta^{18}O$ distributions, and the histogram peaks correlate to high-$\delta^{18}O$, zoned, bright-CL vs. massive or mottled, dark-CL textures. Microquartz, chalcedony and vein megaquartz each exhibit unimodal distributions and have smaller ranges of $\delta^{18}O$ values. None of the chalcedony or quartz showed evidence for significant water in the background corrected OH measurements (Supplementary Fig. 6). Tabulated SIMS data is in Supplementary Table 3.

5. Discussion

The Trendall locality yielded the most variable $\delta^{18}O(Qz)$ of the areas sampled and is the focus of this section. Cammack (2015) reports detailed discussion and interpretation of the Unconformity Ridge and Camel Creek localities.

5.1. Textural and temporal oxygen isotope trends at the Trendall locality

This section discusses the interpreted petrogenetic history of quartz textures at the Trendall locality, coupled with $\delta^{18}O$ analysis at µm-scale according to quartz textural type (Fig. 7, Table 1).

5.1.1. Microquartz and mesoquartz (earliest generation)

Low $\delta^{18}O$ mesoquartz and microquartz not only have similar values of $\delta^{18}O$ but exhibit a grain-diameter continuum without a discrete size-boundary. This suggests that mesoquartz has coarsened from earlier microquartz. Coarsening may have occurred heterogeneously within each sample resulting in microquartz and low $\delta^{18}O$ mesoquartz formation during a single hydrothermal event. Early formation of microquartz and most mesoquartz in the M2 bedded cherts at the Trendall locality is indicated, as these are cut by all other quartz textures (Table 1, Supplementary Fig. 5). Microquartz is also indicated to be an early texture by the fine crystal sizes (< 10 µm). Microquartz has an

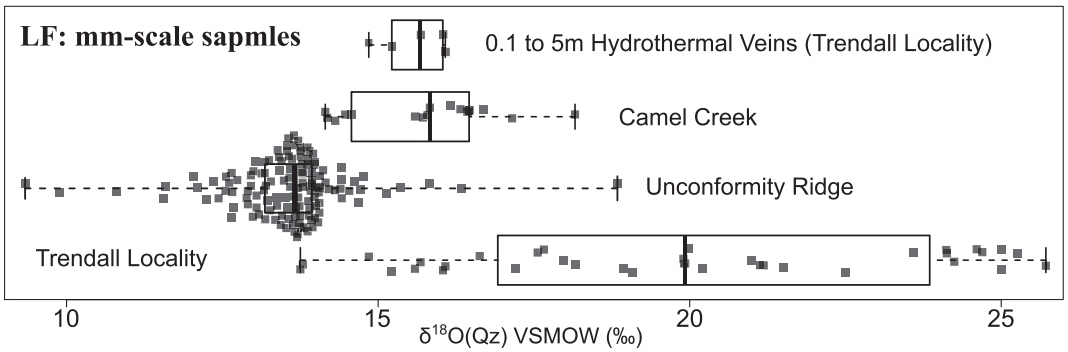

Fig. 6. Boxplot comparing sampling locations $\delta^{18}O$ values at the mm-scale analyzed by laser fluorination. Boxes represent the 2nd and 3rd quartile range of $\delta^{18}O$ for each location. Dark vertical lines are the medians for the data. Whiskers represent the data range for each location. Individual $\delta^{18}O$ points are represented within the boxplot for each locality. See Supplementary Table 2 for tabulated data.

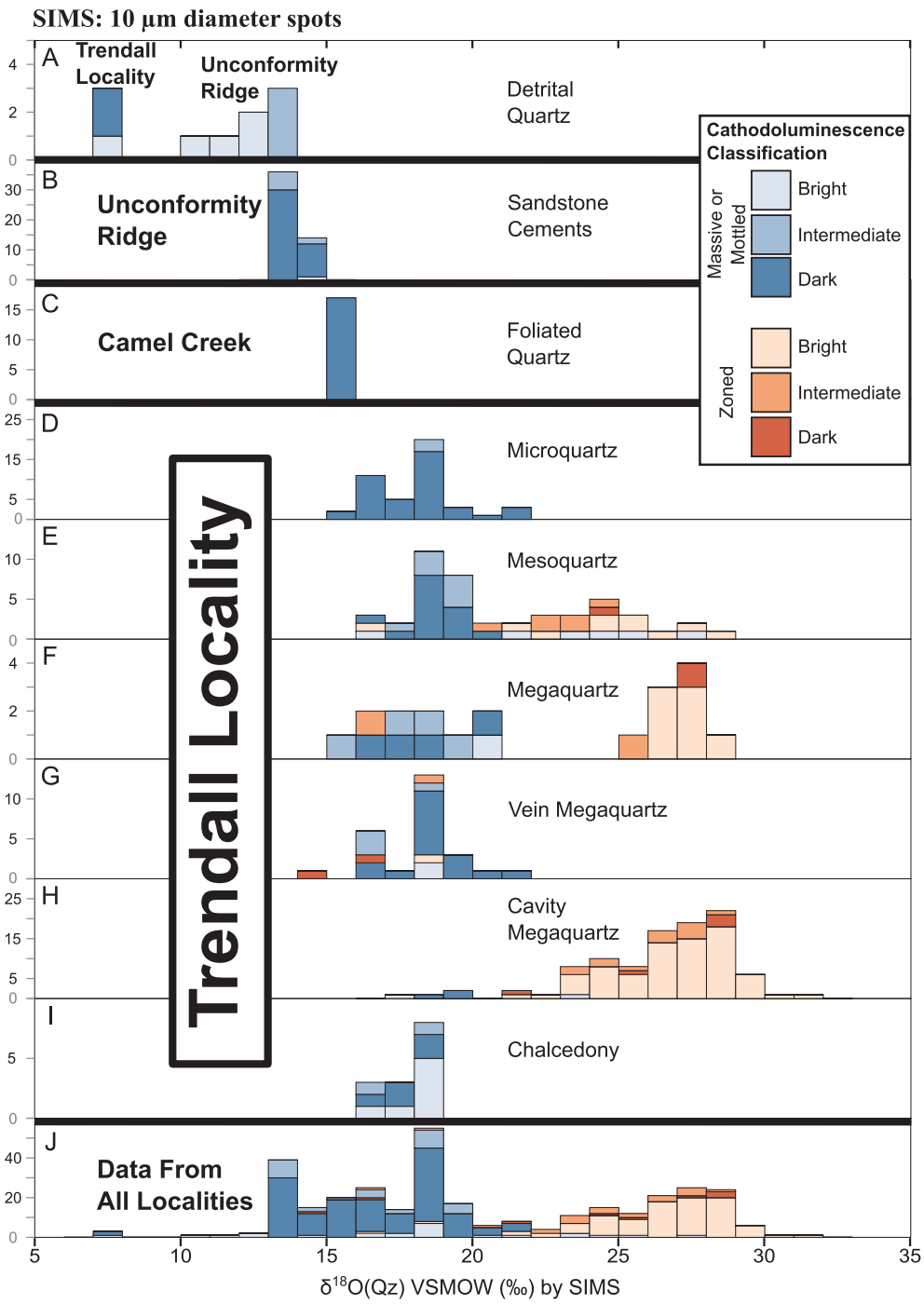

Fig. 7. Histograms of SIMS $\delta^{18}O$ plotted by quartz textures defined by Cross-Polarized Light (XPL) and Cathodoluminescence (CL) analysis. Each histogram indicates a textural classification using either XPL (microquartz, mesoquartz, chalcedony, etc). Warm colors (oranges, red) indicate oscillatory zonation defined by CL, cool colors (blues) indicate mottled or massive CL textures. See Supplementary Table 3 for tabulated data.

average $\delta^{18}O$ of 18.1‰, ranging from 15.6 to 21.9‰, which is similar to vein megaquartz (ave. $\delta^{18}O$ = 18.2‰; range = 14.4–21.2‰) (Fig. 7D and G). Thus, it is possible that vein megaquartz formed after microquartz during early silicification.

Mesoquartz has a bimodal $\delta^{18}O$ distribution: low values are ~16 to 20‰ and high ~21 to 28‰ (Fig. 7E). CL imaging distinguishes these textural types; there is a correlation of bright and zoned textures in the high $\delta^{18}O$ group, versus massive, mostly dark-CL textures in the low $\delta^{18}O$ mesoquartz (Fig. 4B and 7E). On the basis of $\delta^{18}O$ and CL, these low- and high-$\delta^{18}O$ mesoquartz groups are interpreted to have formed in two events: early lower $\delta^{18}O$ hydrothermal alteration, typified by dark-mottled CL, and later high-$\delta^{18}O$ values were related to the formation of cavity megaquartz, typified by bright-zoned CL (as discussed below).

5.1.2. *Megaquartz*

High-$\delta^{18}O$, bright-zoned CL mesoquartz is often adjacent to the basal portions of cavity megaquartz crystals, which grows into voids (Fig. 4B) and has similar $\delta^{18}O$ (Fig. 7E and H). Due to this concentric association surrounding cavity megaquartz, the high $\delta^{18}O$ mesoquartz, which has similar bright and zoned CL textures, is interpreted to have exchanged $\delta^{18}O$ and coarsened through nucleation on what was previously microquartz from the same fluids as cavity megaquartz. Thus, bright-zoned-CL mesoquartz formed contemporaneously with cavity megaquartz and replaced microquartz (Table 1).

Cavity megaquartz and bright, CL-zoned mesoquartz were not observed to be cut by vein megaquartz (Supplementary Fig. 5). Typical euhedral-drusy crystals surrounding and pointing into the center of 50–250 µm cavities (Fig. 5) suggest cavity megaquartz formed after

initial silicification of the SPF carbonates and is the youngest quartz texture at the Trendall locality (Table 1). However, the absolute age of cavity megaquartz could not be established from textural observation. This generation of quartz could have formed from Precambrian hydrothermal fluids or, more recently, during weathering. The cavity megaquartz shows strong oscillatory zonation in CL (Fig. 5B), similar to textures seen in quartz from hydrothermal ore deposits (Rusk et al., 2008) and in diagenetic cements in Paleozoic sandstone (Kelly et al., 2007; Pollington et al., 2016). Cavity megaquartz ranges in $\delta^{18}O$ from 17.9 to 31.3‰ and yields the highest average $\delta^{18}O$ (26.4‰) of any known chert in Archean-deposited sediments (Figs. 1 and 7H). High $\delta^{18}O$ values are also reported for Eocene to Oligocene silcretes in the Lake Eyre Basin from east-central Australia (25–26‰, Alexandre et al., 2004) and for Paleozoic silcretes in Wisconsin (27–32‰, Kelly et al., 2007). Thus, the high $\delta^{18}O$ values and textural occurrence of cavity megaquartz at the Trendall locality are consistent with weathering, which was prevalent in Western Australia in the Cenozoic (Hocking and Cockbain, 1990).

Vein megaquartz cuts all textural categories of quartz except cavity megaquartz and bright, CL-zoned mesoquartz. Therefore, veins form earlier than these textures and later, or penecontemporaneous with earlier quartz textures (e.g. microquartz and dark-CL mesoquartz) (Table 1, Supplementary Fig. 5). Chalcedony (~5 μm thickness) is locally observed in thin section at the edges of quartz veins and thus formed contemporaneously with vein megaquartz. SIMS $\delta^{18}O$ analyses of vein megaquartz range from 14.4 to 21.2‰ (ave. = 18.2‰), similar to microquartz, chalcedony and low-$\delta^{18}O$ mesoquartz suggesting that megaquartz veins formed penecontemporaneously by the same fluids that replaced and silicified SPF carbonates in M2 (Fig. 7D, E, G and I). Field evidence supports this conclusion; hydrothermal veins often interleave with overlying chert units at the Trendall locality and elsewhere in the SPF but do not crosscut the overlying Euro Basalt (Van Kranendonk and Pirajno, 2004; Hickman et al., 2011) (Fig. 3 and Supplementary Fig. 2).

Vein megaquartz in mm-scale veins from the Trendall locality has higher and more variable $\delta^{18}O$ (ave. = 18.2‰; range = 14.4–21.2‰ Fig. 7G) than decimeter- to meter-scale veins (ave. $\delta^{18}O$ = 15.6‰; range = 14.9–16.1‰ Fig. 6). The difference in $\delta^{18}O$ of small vs. large veins is expected if vein fluids cooled as they dispersed into smaller mm-scale conduits while permeating and exchanging with high-$\delta^{18}O$ sediments (Supplementary Fig. 2). Thinner veins had lower fluid fluxes during exchange of low-$\delta^{18}O$ water with high-$\delta^{18}O$ dolomite (dolomite ave. = 18.4‰; Appendix 2 and Supplementary Tables 4 and 6 in Cammack, 2015). Thus, both lower temperatures and mixing would make thinner veins higher in $\delta^{18}O(Qz)$.

5.1.3. Chalcedony

Chalcedony at Trendall has low and unimodal values of $\delta^{18}O$ (ave. = 18.2 ± 1.7‰ 2SD), strengthening the textural association with hydrothermal fluids that also formed vein megaquartz (Fig. 7G and I). Chalcedony is often seen filling cavities and voids. It is observed as a first-stage cavity filling cement due to its occurrence at or near the edges of vein megaquartz. It may have formed by direct precipitation (Heaney, 1993) at the edges of hydrothermal conduits or by re-crystallization of a silica-gel precursor (Oehler, 1976) depending on temperature, crystallization rate, and degree of silica oversaturation (Williams and Crerar, 1985; Xu et al., 1998).

5.1.4. Detrital quartz

Three outlier $\delta^{18}O(Qz)$ analyses from SPF member 2 (M2) cherts at the Trendall locality have $\delta^{18}O \approx 7.5$‰ (Fig. 7A), similar to unaltered igneous quartz (King et al., 2000; Hoefs, 2015). The analyses are from rounded grains set in matrices of microquartz or mesoquartz (01MB35 – Area 2 and 5 from Cammack, 2015 – Appendix 6; CL images). Although detrital sand is rare in M2, it is common in M1 (not exposed at Trendall). For instance, the basal sandstone of the SPF (M1) that is well exposed on Unconformity Ridge is dominated by detrital quartz with zircons from ~3.51 Ga volcanic rocks in the underlying Coonterunah Subgroup (Valley et al., 2015).

5.2. Silicification of carbonate at the Trendall Locality: $\delta^{18}O(Qz)$

Quartz with petrographically early textures in M2 silicified dolomites (microquartz, low $\delta^{18}O$ mesoquartz, chalcedony; Table 1) has the lowest $\delta^{18}O$ values at the Trendall locality (~15–20‰, Fig. 7D, E, I), similar to $\delta^{18}O$ reported in other studies of Archean chert. These values are more than 15‰ lower than quartz formed at equilibrium temperatures of 10–30 °C if $\delta^{18}O(water) = -1$‰ ($\Delta^{18}O(Qz\text{-}H_2O)$ = 36.3–31.7‰, Pollington et al., 2016, Supplementary Fig. 1), and ~10‰ lower than $\delta^{18}O$ of Phanerozoic marine cherts (Fig. 1). Both macroscopic (Supplementary Fig. 2) and microscopic textures at Trendall show that microquartz formed by silicification of carbonate. Detrital-carbonate grains in thin-section appear rarely in M2 (Allwood et al., 2006a), and are likely unrecognizable after silicification.

5.2.1. Bimodal $\delta^{18}O(Qz)$

As discussed earlier, the bimodal values of $\delta^{18}O(Qz)$ measured by SIMS (Fig. 7 J) show a strong correlation with textures imaged by SEM-CL. Quartz with bright CL and well-developed growth zoning (Fig. 5B) has higher values of $\delta^{18}O$ from ~24 to 31‰, and quartz with dark CL and massive or mottled texture has lower values of $\delta^{18}O$ from ~15 to 20‰. These relations lead to a new understanding of the high $\delta^{18}O$ values at Trendall, first discovered by laser fluorination analysis of mm-scale samples and initially interpreted as Archean. The LF data show that values of $\delta^{18}O$ for quartz are higher and more variable at the Trendall locality than Camel Creek, Unconformity Ridge, or any other Archean cherts (Figs. 1 and 6). LF data include values of $\delta^{18}O(Qz)$ up to 25.7‰, that are the highest LF data known for Mesoarchean chert (above the upper limit in Fig. 1). SIMS μm-scale analyses show more variability and even higher values of up to 31.3‰. More importantly, the SIMS data reveal bimodality for the first time in Precambrian cherts. The majority of quartz with bright-zoned-CL and textures indicating late growth has the higher values of $\delta^{18}O$ above 24‰, whereas most of the dark-CL, early quartz has values below 20‰ (Fig. 7).

5.3. Hydrothermal activity vs. metamorphism

Petrographic investigations coupled with SIMS analyses at Trendall reveal $\delta^{18}O(Qz)$ values at mm- to μm-scale that correlate to specific chert textures and preserve μm-scale $\delta^{18}O$ variability that would have been homogenized by metamorphism. In contrast, μm-scale $\delta^{18}O(Qz)$ analyses in cherts from one sample at Camel Creek (Cammack, 2015) are homogenous (15.5 ± 0.3‰ 2SD, N = 17) due to recrystallization during contact metamorphism from the Corunna Downs granite and homogenization of $\delta^{18}O$ at sub-meter-scale at this locality (Fig. 7). Likewise, the LF data over a distance of 400 m at Camel Creek are the least variable in this study (Fig. 6). The cummingtonite-grunerite amphiboles at this locality (Supplementary Fig. 4) suggest this rock could be a silicified mafic rock at high metamorphic grade. Clearly the Trendall locality experienced lower metamorphic grades than Camel Creek.

5.4. The secular-temporal trend of chert $\delta^{18}O$

The apparent secular-temporal trend of $\delta^{18}O$ in chert (Fig. 1) has been debated for over 50 years. In contrast to earlier work, this study resolves multiple generations of chert and show that none of them were precipitated from seawater and thus none of the oxygen isotope compositions reflect Archean seawater conditions. Outcrop evidence shows that dolomite was the primary deposit (in M2) at the Trendall locality, and was replaced by generations of quartz. Paleoarchean silicification by penecontemporaneous hydrothermal activity is indicated by the

presence of hydrothermal chert veins that cut up through, but do not pass above the SPF. Ironically, the highest $\delta^{18}O$(Qz) (cavity megaquartz, Fig. 7H), which would traditionally be considered the best candidate for precipitation from seawater, is the youngest generation, and likely did not even form during the Archean, and certainly did not precipitate in thermal and isotopic equilibrium with seawater. Thus, an alternative explanation for the temporal-secular chert $\delta^{18}O$ trend (Fig. 1) is that it may reflect different formation processes in Archean cherts vs. Phanerozoic cherts.

5.4.1. Phanerozoic cherts

Many Phanerozoic cherts form from biogenic opaline precursors (diatoms, sponge spicules and radiolaria; Maliva et al., 1989). For instance, the Miocene Monterey Formation, California formed by diagenesis of diatomaceous oozes that accumulated on the margins of North America (Behl, 1999). Recrystallization of opaline precursors occurred at low temperature (17–21 °C; Matheney and Knauth, 1993; Behl and Garrison, 1994) and generally result in $\delta^{18}O$ values that are lower than would be in equilibrium with ocean water at seawater temperatures.

5.4.2. Archean cherts

Archean cherts such as those in the Onverwacht Group, South Africa and the Strelley Pool Formation, which are included in the secular $\delta^{18}O$ trend (Fig. 1), are interbedded with volcanic successions that drove complex hydrothermal systems (e.g., Van Kranendonk, 2006). Archean cherts formed in many environments, but the secular chert $\delta^{18}O$ trend in Fig. 1 is heavily weighted toward Archean cherts collected from greenstone belts.

Archean chert in greenstone belts, such as the Strelley Pool Formation and those from the Onverwacht Group, are usually associated with local and/or regional evidence for hydrothermal activity (de Wit et al., 1982, 2011; Paris et al., 1985; Westall et al., 2001; Brown et al., 2004; Van Kranendonk and Pirajno, 2004; Van Kranendonk, 2006). At the Trendall locality, the Strelley Pool Formation is less intensely altered than in most other areas, but has: hydrothermal chert veins that cut across and feed into “bedded” cherts that represent silicified carbonates (Fig. 3 and Supplementary Fig. 2); early microquartz that is similar in $\delta^{18}O$ to quartz veins (Fig. 7); and quartz that has pseudomorphed carbonates (Supplementary Fig. 3). Thus, Trendall locality cherts, excluding the late cavity megaquartz, originated from Paleoarchean hydrothermal activity that was at low temperatures, but distinctly warmer than seawater.

As discussed earlier, comparisons of $\delta^{18}O$ data from cherts of different age (Fig. 1) implicitly assume that they formed in similar conditions. This has evoked considerable debate for 5 decades. Archean cherts in the present study did not precipitate directly from seawater. Numerous studies, have documented Archean cherts that experienced similarly complex, metamorphic, diagenetic, and hydrothermal petrogenetic histories.

6. Conclusions

Detailed petrography and mm- to μm-scale measurements of $\delta^{18}O$ (Qz) lead to a new and more detailed understanding of petrogenesis for “bedded” cherts in the 3.4 Ga Strelley Pool Formation of the Pilbara Craton, Western Australia. Several generations of quartz are recognized and in-situ SIMS analyses reveal that $\delta^{18}O$(Qz) values are variable at the μm-scale and correlate to petrographic textures. Bimodal $\delta^{18}O$ quartz analyses at the Trendall locality (Fig. 7) reveal two events: 1) a Paleoarchean hydrothermal event which formed dark-mottled CL microquartz, mesoquartz, chalcedony and vein quartz with ($\delta^{18}O$ = ~15–20‰); 2) a relatively-recent, post-Archean, weathering event which formed bright, zoned CL cavity megaquartz and mesoquartz with values of uniquely high $\delta^{18}O$ for “Archean” host rocks ($\delta^{18}O$ = ~24–29‰). This richness of information was unknown in earlier studies that homogenized cm- to mm-scale samples for analysis of $\delta^{18}O$ by bulk methods.

Texture-specific, μm-scale $\delta^{18}O$(Qz) values are strongly zoned and $\delta^{18}O$(Qz) values differ at micrometer to kilometer scales in the Strelley Pool Formation. Paleoarchean sedimentary and authigenic features are unusually well preserved at the Trendall locality. Quartz at Trendall has the highest and most variable $\delta^{18}O$ values that have been reported in Archean cherts. At other localities hydrothermal alteration and contact metamorphism were driven by adjacent plutonic and volcanic rocks, and were variable in intensity. By contrast the Strelley Pool Formation at the Trendall locality preserves a low temperature oasis where hydrothermal activity was less intense than at other localities. These cherts preserve massive and stromatolitic dolomite, and relatively elevated $\delta^{18}O$ of early-formed textures (e.g., 15–20‰, microquartz, chalcedony); this differs from the SPF chert at Unconformity Ridge and Camel Creek (10–16‰).

The $\delta^{18}O$ values of earliest formed quartz within the Strelley Pool Formation does not record thermal or isotopic equilibrium with Archean seawater. The quartz in these cherts is seen at m- to μm-scale to replace earlier carbonates. We present a new hypothesis that the $\delta^{18}O$ record shown for chert in Fig. 1 is biased due to the comparison of Archean cherts that may have formed by complex combinations of hydrothermal activity, metamorphism, and diagenetic cements, to younger cherts that mainly formed by diagenetic or biogenic processes in basinal settings. We challenge the traditional interpretations of this trend, and question whether samples in this trend are genuine seawater precipitates, products of hydrothermal activity, diagenetic cements, or a combination thereof. Detailed field observation and petrography coupled to in-situ isotope analysis by SIMS will allow this hypothesis to be tested in other cherts comprising the secular-temporal $\delta^{18}O$ trend.

Acknowledgments

We thank: Brian Hess for casting and polishing SIMS samples; David Valley for assistance in the 2001 Australia field-work; Julie Vry for petrography; Adam Denny and Ben Linzmeier who collaborated in developing QGIS techniques for plotting microanalytical data; Ben Linzmeier and Ryan Quinn who helped coding in 'R'; Maciej Śliwiński for developing ankerite SIMS standards; Andrée Valley who redrafted many of the figures; John Fournelle and Phil Gopon who assisted with EPMA and SEM; and Cody Cammack for her advice and support. Arthur Hickman publishes with permission of the Executive Director of the Geological Survey of Western Australia. This research was funded by the NASA Astrobiology Institute. WiscSIMS is funded by NSF (EAR-1355590) and UW-Madison. This is contribution number 1017 of the Australian Research Council Centre for Excellence for CORE to Crust Fluids, to which Martin Van Kranendonk is grateful for funding support.

Appendix A. Supplementary data

Supplementary data associated with this article can be found, in the online version, at http://dx.doi.org/10.1016/j.precamres.2017.11.005.

References

Alexandre, A., Meunier, J.-D., Llorens, E., Hill, S.M., Savin, S.M., 2004. Methodological improvements for investigating silcrete formation: petrography, FT-IR and oxygen isotope ratio of silcrete quartz cement, Lake Eyre Basin (Australia). Chem. Geol. 211, 261–274. http://dx.doi.org/10.1016/j.chemgeo.2004.06.024.

Allwood, A.C., Walter, M.R., Kamber, B.S., Marshall, C.P., Burch, I.W., 2006a. Stromatolite reef from the Early Archaean era of Australia. Nature 441, 714–718. http://dx.doi.org/10.1038/nature04764.

Allwood, A.C., Walter, M.R., Marshall, C.P., 2006b. Raman spectroscopy reveals thermal palaeoenvironments of c. 3.5 billion-year-old organic matter. Vib. Spectrosc. 41, 190–197. http://dx.doi.org/10.1016/j.vibspec.2006.02.006.

Allwood, A.C., Walter, M.R., Burch, I.W., Kamber, B.S., 2007. 3.43 billion-year-old stromatolite reef from the Pilbara Craton of Western Australia: ecosystem-scale insights to early life on Earth. Precambr. Res. 158, 198–227. http://dx.doi.org/10.1016/j.precamres.2007.04.013.

Baertschi, P., 1976. Absolute ^{18}O content of standard mean ocean water. Earth Planet. Sci.

Lett. 31, 341–344. http://dx.doi.org/10.1016/0012-821X(76)90115-1.
Behl, R.J., Garrison, R.E., 1994. The origin of chert in the Monterey Formation of California (USA). In: Siliceous, phosphatic and glauconitic sediments of the Tertiary and Mesozoic: Proceedings of the 29th International Geological Congress, Part C, pp. 101–132.
Behl, R.J., 1999. Since Bramlette (1946): The Miocene Monterey Formation of California revisited: Classic Cordilleran Concepts: A View from California: Geological Society of America, Special Paper, vol. 338, p. 301–313.
Blake, R.E., Chang, S.J., Lepland, A., 2010. Phosphate oxygen isotopic evidence for a temperate and biologically active Archaean ocean. Nature (London) 464, 1029–1032. http://dx.doi.org/10.1038/nature08952.
Bohrmann, G., Abelmann, A., Gersonde, R., Hubberten, H., Kuhn, G., 1994. Pure siliceous ooze, a diagenetic environment for early chert formation. Geology 22, 207–210. http://dx.doi.org/10.1130/0091-7613(1994)022<0207:PSOADE>2.3.CO;2.
Boorn, S.H.J.M. van den, Bergen, M.J. van, Nijman, W., Vroon, P.Z., 2007. Dual role of seawater and hydrothermal fluids in Early Archean chert formation: evidence from silicon isotopes. Geology 35, 939–942. http://dx.doi.org/10.1130/G24096A.1.
Boorn, S.H.J.M. van den, Bergen, M.J. van, Vroon, P.Z., de Vries, S.T., Nijman, W., 2010. Silicon isotope and trace element constraints on the origin of ~3.5Ga cherts: implications for Early Archaean marine environments. Geochim. Cosmochim. Acta 74, 1077–1103. http://dx.doi.org/10.1016/j.gca.2009.09.009.
Boyd, E.S., Hamilton, T.L., Spear, J.R., Lavin, M., Peters, J.W., 2010. [FeFe]-hydrogenase in Yellowstone National Park: evidence for dispersal limitation and phylogenetic niche conservatism. Int. Soc. Microb. Ecol. J. 4, 1485–1495. http://dx.doi.org/10.1038/ismej.2010.76.
Brasier, M., Green, O., Shields, G., 1997. Ediacaran sponge spicule clusters from southwestern Mongolia and the origins of the Cambrian fauna. Geology 25, 303–306.
Brasier, M., McLoughlin, N., Green, O., Wacey, D., 2006. A fresh look at the fossil evidence for early Archaean cellular life. Philos. Trans. R. Soc. London B: Biol. Sci. 361, 887–902. http://dx.doi.org/10.1098/rstb.2006.1835.
Brasier, M.D., Antcliffe, J., Saunders, M., Wacey, D., 2015. Changing the picture of Earth's earliest fossils (3.5–1.9 Ga) with new approaches and new discoveries. Proc. Natl. Acad. Sci. 112, 4859–4864. http://dx.doi.org/10.1073/pnas.1405338111.
Brock, T.D., Brock, M.L., 1968. Measurement of steady-state growth rates of a thermophilic alga directly in nature. J. Bacteriol. 95, 811–815.
Brown, A., Walter, M., Cudahy, T., 2004. Short-wave infrared reflectance investigation of sites of paleobiological interest: applications for mars exploration. Astrobiology 4, 359–376. http://dx.doi.org/10.1089/ast.2004.4.359.
Brown, A.J., Cudahy, T.J., Walter, M.R., 2006. Hydrothermal alteration at the Panorama formation, North Pole Dome, Pilbara Craton, Western Australia. Precambrian Res. 151, 211–223.
Buick, R., Dunlop, J.S.R., 1990. Evaporitic sediments of Early Archaean age from the Warrawoona Group, North Pole, Western Australia. Sedimentology 37, 247–277. http://dx.doi.org/10.1111/j.1365-3091.1990.tb00958.x.
Buick, R., Dunlop, J.S.R., Groves, D.I., 1981. Stromatolite recognition in ancient rocks: an appraisal of irregularly laminated structures in an Early Archaean chert-barite unit from North Pole, Western Australia. Alcheringa: Aust. J. Palaeontol. 5, 161–181. http://dx.doi.org/10.1080/03115518108566999.
Buick, R., Groves, D.I., Dunlop, J.S.R., Lowe, D.R., 1995. Abiological origin of described stromatolites older than 3.2 Ga: comment and reply. Geology 23, 191–192. http://dx.doi.org/10.1130/0091-7613(1995)023<0191:AOODSO>2.3.CO;2.
Cammack, J.N., 2015. SIMS Microanalysis of the Strelley Pool Formation Cherts and the Implications for the Secular-Temporal Oxygen-isotope Trend of Cherts (MS thesis). University of Wisconsin, Madison p. 206.
Coplen, T.B., 1988. Normalization of oxygen and hydrogen isotope data. Chem. Geol.: Isotope Geosci. Sect. 72, 293–297. http://dx.doi.org/10.1016/0168-9622(88)90042-5.
Cunningham, L.C., Page, F.Z., Simonson, B.M., Kozdon, R., Valley, J.W., 2012. Ion microprobe analyses of $\delta^{18}O$ in early quartz cements from 1.9 Ga granular iron formations (GIFs); a pilot study. Precambrian Res. 214–215, 258–268. http://dx.doi.org/10.1016/j.precamres.2012.01.016.
Dammer, D., McDougall, I., Chivas, A.R., 1999. Timing of weathering-induced alteration of manganese deposits in Western Australia; evidence from K/Ar and $^{40}Ar/^{39}Ar$ dating. Econ. Geol. 94, 87–108. http://dx.doi.org/10.2113/gsecongeo.94.1.87.
de Wit, M.J., Hart, R., Martin, A., Abbott, P., 1982. Archean abiogenic and probable biogenic structures associated with mineralized hydrothermal vent systems and regional metasomatism, with implications for greenstone belt studies. Econ. Geol. 77, 1783–1802.
de Wit, M.J., Furnes, H., Robins, B., 2011. Geology and tectonostratigraphy of the Onverwacht Suite, Barberton Greenstone Belt, South Africa. Precambrian Res. 186, 1–27. http://dx.doi.org/10.1016/j.precamres.2010.12.007.
Degens, E.T., Epstein, S., 1962. Relationship between O^{18}/O^{16} ratios in coexisting carbonates, cherts, and diatomites. Am. Assoc. Petrol. Geol. Bull. 46, 534–542.
Degens, E.T., Epstein, S., 1964. Oxygen and carbon isotope ratios in coexisting calcites and dolomites from recent and ancient sediments. Geochim. Cosmochim. Acta 28, 23–44. http://dx.doi.org/10.1016/0016-7037(64)90053-5.
Duda, J.-P., Kranendonk, M.J.V., Thiel, V., Ionescu, D., Strauss, H., Schäfer, N., Reitner, J., 2016. A rare glimpse of paleoarchean life: geobiology of an exceptionally preserved microbial mat facies from the 3.4 Ga Strelley Pool formation, Western Australia. PLoS ONE 11, e0147629. http://dx.doi.org/10.1371/journal.pone.0147629.
Folk, R.L., 1980. Petrology of Sedimentary Rocks. Hemphill Publ. Co., Austin, TX. 184 p, http://search.proquest.com.ezproxy.library.wisc.edu/georef/docview/51770806/2713EEAD1C274B95PQ/1?accountid=465 (accessed June 2015).
Folk, R.L., Weaver, C.E., 1952. A study of the texture and composition of chert. Am. J. Sci. 250, 498–510. http://dx.doi.org/10.2475/ajs.250.7.498.
Gregory, R.T., 1991. Oxygen isotope history of seawater revisited; timescales for boundary event changes in the oxygen isotope composition of seawater. In: Taylor H. P., O'Neil J.R., I. R. Kaplan (Eds.), Special Publication – Geochemical Society, vol. 3, pp. 65–76.
Gunnarsson, I., Arnórsson, S., 2000. Amorphous silica solubility and the thermodynamic properties of H_4SiO_4 in the range of 0° to 350 °C at P_{sat}. Geochim. Cosmochim. Acta 64, 2295–2307. http://dx.doi.org/10.1016/S0016-7037(99)00426-3.
Hamilton, T.L., Vogl, K., Bryant, D.A., Boyd, E.S., Peters, J.W., 2012. Environmental constraints defining the distribution, composition, and evolution of chlorophototrophs in thermal features of Yellowstone National Park. Geobiology 10, 236–249. http://dx.doi.org/10.1111/j.1472-4669.2011.00296.x.
Heaney, P.J., 1993. A proposed mechanism for the growth of chalcedony. Contrib. Miner. Petrol. 115, 66–74. http://dx.doi.org/10.1007/BF00712979.
Hein, J.R., Yeh, H.W., 1983. Oxygen-Isotope Composition of Secondary Silica Phases, Costa-Rica Rift Deep-Sea Drilling Project Leg-69. Init. Rep. Deep Sea Drilling Proj. 69, 423–429.
Hervig, R.L., 1992. Oxygen isotope analysis using extreme energy filtering. Chem. Geol.: Isotope Geosci. Sect. 101, 185–186. http://dx.doi.org/10.1016/0009-2541(92)90216-R.
Hickman, A.H., Van Kranendonk, M.J., Grey, K., 2011. State Geoheritage Reserve R50149 (Trendall Reserve), Geology and Evidence for Early Archean Life: GSWA Record 2011/10, p. 32.
Hickman, A.H., 2008. Regional review of the 3426-3350 Ma Strelley Pool Formation, Pilbara Craton, Western Australia: Geological Survey of Western Australia, Record 2008/15, p. 27.
Hocking, R.M., Cockbain, A.E., 1990. Regolith, in Geology and Mineral Resources of Western Australia: Geological Survey of Western Australia. Memoir 3, 591–601.
Hoefs, J., 2015. Stable Isotope Geochemistry, 7th ed. Springer. p. 389, http://link.springer.com/chapter/10.1007/978-3-319-19716-6_2.
Hofmann, H.J., Grey, K., Hickman, A.H., Thorpe, R.I., 1999. Origin of 3.45 Ga coniform stromatolites in Warrawoona Group, Western Australia. Geol. Soc. Am. Bull. 111, 1256–1262. http://dx.doi.org/10.1130/0016-7606(1999)111<1256:OOGCSI>2.3.CO;2.
Holness, M.B., Watt, G.R., 2001. Quartz recrystallization and fluid flow during contact metamorphism: a cathodoluminescence study. Geofluids 1, 215–228. http://dx.doi.org/10.1046/j.1468-8123.2001.00015.x.
Jacob, D., Jagoutz, E., Lowry, D., Mattey, D., Kudrjavtseva, G., 1994. Diamondiferous eclogites from Siberia: remnants of Archean oceanic crust. Geochim. Cosmochim. Acta 58, 5191–5207. http://dx.doi.org/10.1016/0016-7037(94)90304-2.
Jacob, D.E., 2004. Nature and origin of eclogite xenoliths from kimberlites. Lithos 77, 295–316. http://dx.doi.org/10.1016/j.lithos.2004.03.038.
Jaffrés, J.B.D., Shields, G.A., Wallmann, K., 2007. The oxygen isotope evolution of seawater: a critical review of a long-standing controversy and an improved geological water cycle model for the past 3.4 billion years. Earth Sci. Rev. 83, 83–122. http://dx.doi.org/10.1016/j.earscirev.2007.04.002.
Jehlička, J., Urban, O., Pokorný, J., 2003. Raman spectroscopy of carbon and solid bitumens in sedimentary and metamorphic rocks. Spectrochim. Acta Part A Mol. Biomol. Spectrosc. 59, 2341–2352. http://dx.doi.org/10.1016/S1386-1425(03)00077-5.
Karhu, J., Epstein, S., 1986. The implication of the oxygen isotope records in coexisting cherts and phosphates. Geochim. Cosmochim. Acta 50, 1745–1756. http://dx.doi.org/10.1016/0016-7037(86)90136-5.
Kasting, J.F., Howard, M.T., Wallmann, K., Veizer, J., Shields, G., Jaffrés, J., 2006. Paleoclimates, ocean depth, and the oxygen isotopic composition of seawater. Earth Planet. Sci. Lett. 252, 82–93. http://dx.doi.org/10.1016/j.epsl.2006.09.029.
Kasting, J.F., 1993. Earth's early atmosphere. Science 259, 920–926.
Kastner, M., Keene, J.B., Gieskes, J.M., 1977. Diagenesis of siliceous oozes—I. Chemical controls on the rate of opal-A to opal-CT transformation—an experimental study. Geochim. Cosmochim. Acta 41, 1041–1059. http://dx.doi.org/10.1016/0016-7037(77)90099-0.
Keene, J.B., 1975. Cherts and porcellanites from the North Pacific, DSDP Leg 32. Init. Rep. Deep Sea Drilling Proj. 32, 429–507.
Kelly, J.L., Fu, B., Kita, N.T., Valley, J.W., 2007. Optically continuous silcrete quartz cements of the St. Peter Sandstone: high precision oxygen isotope analysis by ion microprobe. Geochim. Cosmochim. Acta 71, 3812–3832. http://dx.doi.org/10.1016/j.gca.2007.05.014.
King, E.M., Valley, J.W., Davis, D.W., 2000. Oxygen isotope evolution of volcanic rocks at the Sturgeon Lake volcanic complex, Ontario. Can. J. Earth Sci. 37, 39–50. http://dx.doi.org/10.1139/e99-106.
Kita, N.T., Ushikubo, T., Fu, B., Valley, J.W., 2009. High precision SIMS oxygen isotope analysis and the effect of sample topography. Chem. Geol. 264, 43–57. http://dx.doi.org/10.1016/j.chemgeo.2009.02.012.
Knauth, L.P., Epstein, S., 1976. Hydrogen and oxygen isotope ratios in nodular and bedded cherts. Geochim. Cosmochim. Acta 40, 1095–1108. http://dx.doi.org/10.1016/0016-7037(76)90051-X.
Knauth, L.P., Lowe, D.R., 2003. High Archean climatic temperature inferred from oxygen isotope geochemistry of cherts in the 3.5 Ga Swaziland Supergroup, South Africa. Geol. Soc. Am. Bull. 115, 566–580. http://dx.doi.org/10.1130/0016-7606(2003)1150566:HACTIF2.0.CO;2.
Knauth, L.P., 1992. Origin and diagenesis of cherts: an isotopic perspective. In: Clauer, N., Chaudhuri, S. (Eds.), Isotopic Signatures and Sedimentary Records. Lecture Notes in Earth Sciences, vol. 43 Springer, Berlin Heidelberg. pp. 123–152, http://link.springer.com/chapter/10.1007/BFb0009863.
Knauth, L.P., 1994. Petrogenesis of chert. Rev. Mineral. 29, 233–258.
Knauth, L.P., 2005. Temperature and salinity history of the Precambrian ocean: implications for the course of microbial evolution. Palaeogeogr., Palaeoclimatol.,

Palaeoecol. 219, 53–69. http://dx.doi.org/10.1016/j.palaeo.2004.10.014.
Kozdon, R., Kita, N.T., Huberty, J.M., Fournelle, J.H., Johnson, C.A., Valley, J.W., 2010. In situ sulfur isotope analysis of sulfide minerals by SIMS: precision and accuracy, with application to thermometry of ~3.5 Ga Pilbara cherts. Chem. Geol. 275, 243–253. http://dx.doi.org/10.1016/j.chemgeo.2010.05.015.
Lepot, K., Williford, K.H., Ushikubo, T., Sugitani, K., Mimura, K., Spicuzza, M.J., Valley, J.W., 2013. Texture-specific isotopic compositions in 3.4 Gyr old organic matter support selective preservation in cell-like structures. Geochim. Cosmochim. Acta 112, 66–86. http://dx.doi.org/10.1016/j.gca.2013.03.004.
Li, W., Johnson, C.M., Beard, B.L., 2012. U-Th-Pb isotope data indicate Phanerozoic age for oxidation of the 3.4 Ga Apex Basalt. Earth Planet. Sci. Lett. 319–320, 197–206. http://dx.doi.org/10.1016/j.epsl.2011.12.035.
Lindsay, J.F., Brasier, M.D., McLoughlin, N., Green, O.R., Fogel, M., Steele, A., Mertzman, S.A., 2005. The problem of deep carbon—an Archean paradox. Precambr. Res. 143, 1–22. http://dx.doi.org/10.1016/j.precamres.2005.09.003.
Lowe, D.R., 1983. Restricted shallow-water sedimentation of early Archean stromatolitic and evaporitic strata of the Strelley Pool Chert, Pilbara Block, Western Australia. Precambrian Res. 19, 239–283.
Lowe, D.R., 1994. Abiological origin of described stromatolites older than 3.2 Ga. Geology 22, 387–390. http://dx.doi.org/10.1130/0091-7613(1994)022<0387:AOODSO>2.3.CO;2.
Maliva, R.G., Knoll, A.H., Siever, R., 1989. Secular change in chert distribution: a reflection of evolving biological participation in the silica cycle. Palaios 519–532.
Maliva, R.G., Knoll, A.H., Simonson, B.M., 2005. Secular change in the Precambrian silica cycle: insights from chert petrology. Geol. Soc. Am. Bull. 117, 835–845. http://dx.doi.org/10.1130/B25555.1.
Marin, J., Chaussidon, M., Robert, F., 2010. Microscale oxygen isotope variations in 1.9 Ga Gunflint cherts: assessments of diagenesis effects and implications for oceanic paleotemperature reconstructions. Geochim. Cosmochim. Acta 74, 116–130. http://dx.doi.org/10.1016/j.gca.2009.09.016.
Marin-Carbonne, J., Robert, F., Chaussidon, M., 2014. The silicon and oxygen isotope compositions of Precambrian cherts; a record of oceanic paleotemperatures? Precambr. Res. 247, 223–234. http://dx.doi.org/10.1016/j.precamres.2014.03.016.
Matheney, R.K., Knauth, L.P., 1993. New isotopic temperature estimates for early silica diagenesis in bedded cherts. Geology 21, 519–522. http://dx.doi.org/10.1130/0091-7613(1993)021<0519:NITEFE>2.3.CO;2.
Muehlenbachs, K., 1998. The oxygen isotopic composition of the oceans, sediments and the seafloor. Chem. Geol. 145, 263–273. http://dx.doi.org/10.1016/S0009-2541(97)00147-2.
Murata, K.J., Nakata, J.K., 1974. Cristobalitic stage in the diagenesis of diatomaceous shale. Science 184, 567–568.
Nelson, D.R., 1998. 142836: volcaniclastic sedimentary rock, Gorge Creek; Geochronology dataset 393393; in Compilation of geochronology data, June 2007 update, Geological Survey of Western Australia.
Nhleko, N., 2003. The Pongola Supergroup in Swaziland. Rand Afrikaans University. http://ujdigispace.uj.ac.za/handle/10210/1966.
Oehler, J.H., 1976. Hydrothermal crystallization of silica gel. Geol. Soc. Am. Bull. 87, 1143–1152. http://dx.doi.org/10.1130/0016-7606(1976)87<1143:HCOSG>2.0.CO;2.
Paris, I., Stanistreet, I.G., Hughes, M.J., 1985. Cherts of the Barberton greenstone belt interpreted as products of submarine exhalative activity. J. Geol. 111–129.
Perry Jr., E.C., Lefticariu, L., 2007. Formation and Geochemistry of Precambrian Cherts. In: Turekian, K.K., Holland, H.D. (Eds.), Treatise on Geochemistry. Pergamon, Oxford, pp. 1–21. http://www.sciencedirect.com/science/article/pii/B0080437516071383.
Perry, E.C., Tan, F.C., 1972. Significance of oxygen and carbon isotope variations in early precambrian cherts and carbonate rocks of Southern Africa. Geol. Soc. Am. Bull. 83, 647–664. http://dx.doi.org/10.1130/0016-7606(1972)83[647:SOOACI]2.0.CO;2.
Pollington, A.D., Kozdon, R., Anovitz, L.M., Georg, R.B., Spicuzza, M.J., Valley, J.W., 2016. Experimental calibration of silicon and oxygen isotope fractionations between quartz and water at 250 & #xB0;C by in situ microanalysis of experimental products and application to zoned low δ30Si quartz overgrowths. Chem. Geol. 421, 127–142. http://dx.doi.org/10.1016/j.chemgeo.2015.11.011.
Prokoph, A., Shields, G.A., Veizer, J., 2008. Compilation and time-series analysis of a marine carbonate $\delta^{18}O$, $\delta^{13}C$, $^{87}Sr/^{86}Sr$ and $\delta^{34}S$ database through Earth history. Earth Sci. Rev. 87, 113–133. http://dx.doi.org/10.1016/j.earscirev.2007.12.003.
QGIS Development Team, 2014. QGIS Geographic Information System: Open Source Geospatial Foundation Project, http://qgis.osgeo.org/en/site/.
Riech, V., von Rad, U., 1979. Silica Diagenesis in the Atlantic Ocean: Diagenetic Potential and Transformations. In: Talwani, Manik, W. Hay, W.B.F. Ryan (Eds.), Deep Drilling Results in the Atlantic Ocean: Continental Margins and Paleoenvironment, American Geophysical Union, pp. 315–340, http://onlinelibrary.wiley.com.ezproxy.library.wisc.edu/doi/10.1029/ME003p0315/summary.
Robert, F., Chaussidon, M., 2006. A palaeotemperature curve for the Precambrian oceans based on silicon isotopes in cherts. Nature 443, 969–972. http://dx.doi.org/10.1038/nature05239.
Rouchon, V., Orberger, B., 2008. Origin and mechanisms of K-Si-metasomatism of ca. 3.4-3.3 Ga volcaniclastic deposits and implications for Archean seawater evolution: examples from cherts of Kittys Gap (Pilbara craton, Australia) and Msauli (Barberton Greenstone Belt, South Africa). Precambr. Res. 165, 169–189. http://dx.doi.org/10.1016/j.precamres.2008.06.003.
Rusk, B.G., Lowers, H.A., Reed, M.H., 2008. Trace elements in hydrothermal quartz: relationships to cathodoluminescent textures and insights into vein formation. Geology 36, 547–550. http://dx.doi.org/10.1130/G24580A.1.
Sagan, C., Mullen, G., 1972. Earth and mars: evolution of atmospheres and surface temperatures. Science 177, 52–56. http://dx.doi.org/10.1126/science.177.4043.52.
Schwartzman, D.W., Knauth, P., Meech, K.J., Boss, A., Irvine, W., 2007. A hot climate on early Earth; implications to biospheric evolution. Astrobiology 7, 494. http://dx.doi.org/10.1089/ast.2007.1016.
Shields, G.A., 2007. Chapter 7.6 The Marine Carbonate and Chert Isotope Records and Their Implications for Tectonics, Life and Climate on the Early Earth. In: Van Kranendonk, Martin J., Bennett, Vickie, Smithies, Hugh (Eds.), Developments in Precambrian Geology. Earth's Oldest Rocks, vol. 15 Elsevier. pp. 971–983, http://www.sciencedirect.com/science/article/pii/S0166263507150763.
Shields, G., Veizer, J., 2002. Precambrian marine carbonate isotope database; Version 1.1. Geochem. Geophys. Geosyst. - G3 3. http://dx.doi.org/10.1029/2001GC000266.
Shirey, S.B., Richardson, S.H., 2011. Start of the Wilson cycle at 3 Ga shown by diamonds from subcontinental mantle. Science 333, 434–436.
Siever, R., 1992. The silica cycle in the Precambrian. Geochim. Cosmochim. Acta 56, 3265–3272. http://dx.doi.org/10.1016/0016-7037(92)90303-Z.
Spicuzza, M.J., Valley, J.W., Kohn, M.J., Girard, J.P., Fouillac, A.M., 1998. The rapid heating, defocused beam technique: a CO_2-laser-based method for highly precise and accurate determination of $\delta^{18}O$ values of quartz. Chem. Geol. 144, 195–203. http://dx.doi.org/10.1016/S0009-2541(97)00131-9.
Sugitani, K., Yamashita, F., Nagaoka, T., Yamamoto, K., Minami, M., Mimura, K., Suzuki, K., 2006. Geochemistry and sedimentary petrology of Archean clastic sedimentary rocks at Mt. Goldsworthy, Pilbara Craton, Western Australia: evidence for the early evolution of continental crust and hydrothermal alteration. Precambrian Res. 147, 124–147. http://dx.doi.org/10.1016/j.precamres.2006.02.006.
Sugitani, K., Mimura, K., Nagaoka, T., Lepot, K., Takeuchi, M., 2013. Microfossil assemblage from the 3400 Ma Strelley Pool Formation in the Pilbara Craton, Western Australia: Results form a new locality. Precambrian Res. 226, 59–74. http://dx.doi.org/10.1016/j.precamres.2012.11.005.
Sugitani, K., Mimura, K., Takeuchi, M., Yamaguchi, T., Suzuki, K., Senda, R., Asahara, Y., Wallis, S., Van Kranendonk, M.J., 2015. A Paleoarchean coastal hydrothermal field inhabited by diverse microbial communities: the Strelley Pool Formation, Pilbara Craton, Western Australia. Geobiology 13, 522–545.
Summer, N.S., Ayalon, A., 1995. Dike intrusion into unconsolidated sandstone and the development of quartzite contact zones. J. Struct. Geol. 17, 997–1010. http://dx.doi.org/10.1016/0191-8141(95)00009-3.
Tartèse, R., Chaussidon, M., Gurenko, A., Delarue, F., Robert, F., 2017. Warm Archaean oceans reconstructed from oxygen isotope composition of early-life remnants. Geochem. Perspect. Lett. 55–65. http://dx.doi.org/10.7185/geochemlet.1706.
Terabayashi, M., Masada, Y., Ozawa, H., 2003. Archean Ocean-floor Metamorphism in the North Pole area, Pilbara Craton, Western Australia. Precambrian Res. 127, 167–180. http://dx.doi.org/10.1016/S0301-9268(03)00186-4.
Valley, J.W., Graham, C.M., 1996. Ion microprobe analysis of oxygen isotope ratios in quartz from Skye granite: healed micro-cracks, fluid flow, and hydrothermal exchange. Contrib. Miner. Petrol. 124, 225–234. http://dx.doi.org/10.1007/s004100050188.
Valley, J.W., Kita, N.T., 2009. In situ oxygen isotope geochemistry by ion microprobe: Mineralogical Association of Canada short course: secondary ion mass spectrometry in the earth sciences, 41, pp. 19–63.
Valley, J.W., Kitchen, N., Kohn, M.J., Niendorf, C.R., Spicuzza, M.J., 1995. UWG-2, a garnet standard for oxygen isotope ratios: strategies for high precision and accuracy with laser heating. Geochim. Cosmochim. Acta 59, 5223–5231. http://dx.doi.org/10.1016/0016-7037(95)00386-X.
Valley, J.W., Lackey, J.S., Cavosie, A.J., Clechenko, C.C., Spicuzza, M.J., Basei, M.A.S., Bindeman, I.N., Ferreira, V.P., Sial, A.N., King, E.M., Peck, W.H., Sinha, A.K., Wei, C.S., 2005. 4.4 billion years of crustal maturation: oxygen isotope ratios of magmatic zircon. Contrib. Miner. Petrol. 150, 561–580. http://dx.doi.org/10.1007/s00410-005-0025-8.
Valley, J.W., Spicuzza, M.J., Cammack, J.N., Kitajima, K., Kita, N.T., Van Kranendonk, M. J., 2015. Maturity of Archean Sandstones & Ancient Detrital Zircons: Goldschmidt Abstracts, p. 3220.
Van Kranendonk, M.J., Hickman, A.H., 2000. Archaean geology of the North Shaw region, East Pilbara granite-greenstone terrane, Western Australia – a field guide: Geological Survey of Western Australia, Record 2000/5, p. 64.
Van Kranendonk, M.J., Pirajno, F., 2004. Geochemistry of metabasalts and hydrothermal alteration zones associated with c. 3.45 Ga chert and barite deposits: implications for the geological setting of the Warrawoona Group, Pilbara Craton, Australia. Geochem., Explor., Environ., Anal. 4, 253–278.
Van Kranendonk, M.J., Hickman, A.H., Williams, I.R., Nijman, W., 2001. Archaean geology of the east Pilbara granite-greenstone terrane, Western Australia – a field guide, v. Record 2001/9, p. 134.
Van Kranendonk, M.J., Hickman, A.H., Smithies, R.H., Nelson, D.R., 2002. Geology and tectonic evolution of the Archean North Pilbara Terrain, Pilbara Craton, Western Australia (D. L. Houston, Ed.). Econ. Geol. Bull. Soc. Econ. Geol. 97, 695–732.
Van Kranendonk, M.J., Webb, G.E., Kamber, B.S., 2003. Geological and trace element evidence for a marine sedimentary environment of deposition and biogenicity of 3.45 Ga stromatolitic carbonates in the Pilbara Craton, and support for a reducing Archaean ocean. Geobiology 1, 91–108.
Van Kranendonk, M.J., 2000, Geology of the North Shaw 1: 100 000 sheet: Geological Survey of Western Australia, 1:100 000 Geological Series Explanatory Notes, 86 p.
Van Kranendonk, M.J., 2006. Volcanic degassing, hydrothermal circulation and the flourishing of early life on Earth: a review of the evidence from c. 3490–3240 Ma rocks of the Pilbara Supergroup, Pilbara Craton, Western Australia. Earth-Sci. Rev. 74, 197–240. http://dx.doi.org/10.1016/j.earscirev.2005.09.005.
Van Kranendonk, M.J., 2011. Stromatolite morphology as an indicator of biogenicity for Earth's oldest fossils from the 3.5-3.4 Ga Pilbara Craton, Western Australia. In: Reitner, J., Queric, N.-V., Arp, G. (Eds.), Advances in Stromatolite Geobiology. Lecture Notes in Earth Sciences, vol. 131 Springer, Germany pp. 517–534.

Veizer, J., Hoefs, J., 1976. The nature of O^{18}/O^{16} and C^{13}/C^{12} secular trends in sedimentary carbonate rocks. Geochim. Cosmochim. Acta 40, 1387–1395. http://dx.doi.org/10.1016/0016-7037(76)90129-0.

Veizer, J., Ala, D., Azmy, K., Bruckschen, P., Buhl, D., Bruhn, F., Carden, G.A.F., Diener, A., Ebneth, S., Godderis, Y., Jasper, T., Korte, C., Pawellek, F., Podlaha, O.G., et al., 1999. $^{87}Sr/^{86}Sr$, $\delta^{13}C$ and $\delta^{18}O$ evolution of Phanerozoic seawater. Chem. Geol. 161, 59–88. http://dx.doi.org/10.1016/S0009-2541(99)00081-9.

Wacey, D., McLoughlin, N., Stoakes, C.A., Kilburn, M.R., Green, O.R., Brasier, M.D., 2010. The 3426-3350 Ma Strelley Pool Formation in the East Strelley greenstone belt; a field and petrographic guide: Geological Survey of Western Australia, Record 2010/10, p. 64.

Wacey, D., Kilburn, M.R., Saunders, M., Cliff, J., Brasier, M.D., 2011a. Microfossils of sulphur-metabolizing cells in 3.4-billion-year-old rocks of Western Australia. Nat. Geosci. 4, 698–702. http://dx.doi.org/10.1038/ngeo1238.

Wacey, D., Saunders, M., Brasier, M.D., Kilburn, M.R., 2011b. Earliest microbially mediated pyrite oxidation in ~3.4 billion-year-old sediments. Earth Planet. Sci. Lett. 301, 393–402. http://dx.doi.org/10.1016/j.epsl.2010.11.025.

Walker, J.C.G., Lohmann, K.C., 1989. Why the oxygen isotopic composition of sea water changes with time. Geophys. Res. Lett. 16, 323–326. http://dx.doi.org/10.1029/GL016i004p00323.

Wang, X., Hu, S., Gan, L., Wiens, M., Müller, W.E.G., 2010. Sponges (Porifera) as living metazoan witnesses from the Neoproterozoic: biomineralization and the concept of their evolutionary success. Terra Nova 22, 1–11. http://dx.doi.org/10.1111/j.1365-3121.2009.00909.x.

Wang, X.-L., Coble, M.A., Valley, J.W., Shu, X.-J., Kitajima, K., Spicuzza, M.J., Sun, T., 2014. Influence of radiation damage on Late Jurassic zircon from southern China: evidence from in situ measurements of oxygen isotopes, laser Raman, U-Pb ages, and trace elements. Chem. Geol. 389, 122–136.

Wenzel, B., Lécuyer, C., Joachimski, M.M., 2000. Comparing oxygen isotope records of Silurian calcite and phosphate—$\delta^{18}O$ compositions of brachiopods and conodonts. Geochim. Cosmochim. Acta 64, 1859–1872. http://dx.doi.org/10.1016/S0016-7037(00)00337-9.

Westall, F., de Wit, M.J., Dann, J., van der Gaast, S., de Ronde, C.E.J., Gerneke, D., 2001. Early Archean fossil bacteria and biofilms in hydrothermally-influenced sediments from the Barberton greenstone belt, South Africa. Precambrian Res. 106, 93–116. http://dx.doi.org/10.1016/S0301-9268(00)00127-3.

Williams, L.A., Crerar, D.A., 1985. Silica diagenesis; II, General mechanisms. J. Sediment. Res. 55, 312–321. http://dx.doi.org/10.1306/212F86B1-2B24-11D7-8648000102C1865D.

Williams, G.E., Schmidt, P.W., 1997. Paleomagnetism of the Paleoproterozoic Gowganda and Lorrain formations, Ontario: low paleolatitude for Huronian glaciation. Earth Planet. Sci. Lett. 153, 157–169. http://dx.doi.org/10.1016/S0012-821X(97)00181-7.

Wopenka, B., Pasteris, J.D., 1993. Structural characterization of kerogens to granulite-facies graphite: applicability of Raman microprobe spectroscopy. Am. Mineral. 78, 533–557.

Xu, H., Buseck, P.R., Luo, G., 1998. HRTEM investigation of microstructures in length-slow chalcedony. Am. Mineral. 83, 542–545.

Young, G.M., von Brunn, V., Gold, D.J.C., Minter, W.E.L., 1998. Earth's oldest reported glaciation: physical and chemical evidence from the Archean Mozaan group (~2.9 Ga) of South Africa. J. Geol. 106, 523–538. http://dx.doi.org/10.1086/516039.